LU-TP 21-24
June 2021

The impact of initial state radiation on jets from PbPb collisions

Hilmi Kycyku

Department of Astronomy and Theoretical Physics, Lund University

Bachelor thesis supervised by Korinna Zapp

LUND
UNIVERSITY

Abstract

This thesis presents the study of how initial state radiation impacts jets produced in pp and PbPb collisions, by investigating the transverse momentum spectra, the rapidity spectra and the differential jet shape. This is done for central collisions with $\sqrt{s_{NN}} = 2.76$ TeV and $\sqrt{s_{NN}} = 5.02$ TeV. The anti-k_t algorithm is used to reconstruct the jet, with the jet radii $R = 0.3$ and $R = 1.0$. Further, this thesis investigates to what extent initial state radiation can be separated from medium response on the jet. This is done by analysing events where medium response is included and events where it is not. The results show that the initial state contribution to the jet p_T is quite small. It is larger for low p_T-jets (100-300 GeV) and decreases rapidly for increasing p_T. The initial state contribution also increases for higher rapidity, reaching quite sizeable fractions for e.g. $y = 2.5$. It is also shown that, for PbPb collisions, the initial state contribution is larger for jets with higher jet radius (i.e. R = 1.0) and collisions where $\sqrt{s_{NN}}$ is higher. However, the medium response contribution will also be higher for larger jet radii and beam energy, making it hard to discern the medium response from the initial state contribution.

Populärvetenskaplig beskrivning

Ständigt genom historien, har människan varit intresserad av att försöka bryta ner naturens lagar och fenomen till så fundamentala principer som är möjligt. Redan i antika grekland uppstod konceptet av en fundamental byggsten som uppgör all annan materia. Med en ständigt förbättrande teknik och mer utvecklade teorier, så har man under de senaste 100 åren kunnat undersöka mindre och mindre längdskalor. Detta har resulterat i att man har upptäckt att det finns en mängd fundamentala partiklar med olika egenskaper. De fundamentala partiklarna och deras interaktioner med varandra har samlats i en enda grundläggande model som kallas för Standardmodellen.
Standardmodellen delar upp de fundamentala partiklarna i två grupper, nämligen fermioner och bosoner, beroende på vilket spinn partiklarna har. All materia i universum utgörs av fermioner medan bosonerna är de partiklar som fermionerna (och även vissa bosoner) använder för att växelverka med varandra. Växelverkan sker genom ett utbytte av bosoner som resulterar i att partiklarnas energier och rörelsemängd förändras. I standardmodellen är det tre fundamentala krafter som kan påverka fermionerna. De tre krafterna är elektromagnetismen, den svaga kraften och den starka kraften. Partiklar som har en viss kraftladdning kan alltså interagera med en kraft relaterad till den laddningen. Exempel är då den elektriska laddningen som medför i att partiklar kan växelverka genom den elektromagnetiska kraften.
Fermionerna kan delas in ytterligare i kvarkar och leptoner. Den största skillnaden mellan dessa är att kvarkarna kan växelverka genom den starka kraften, medan leptonerna inte kan det. Detta beror på att kvarkar har en färgladdning, vilket är den laddning som behövs för att växelverka med den starka kraften. Den starka kraften är den starkaste utav de fundamentala krafterna och är ansvarig för skapandet av stora sammansatta partiklar, som är kallade för hadroner. Detta görs genom att gluoner, det vill säga de bosoner som används för att förmedla den starka kraften, binder ihop kvarkarna till ett stabilt objekt. Exempel på hadroner är då protoner eller neutroner. En intressant egenskap med just gluonen är att de också har en färgladdning. Detta är unikt bland de fundamentala krafterna och innebär alltså att gluonerna kan växelverka med varandra. En konsekvens som följer av gluonens självinteraktion är att kvarkarna och gluonerna aldrig kan existera isolerade. De måste alltid vara i färgneutrala tillstånd, tillsammans med andra kvarkar och gluoner.
I partikelacceleratorn LHC (Large Hadron Collider) på CERN, Genève, kolliderar man partiklar med extremt höga energier. Detta möjliggör för skapandet av nya partiklar som då kan studeras med hjälp av olika tekniker och detekorer. De enskilda partiklarna som har skapats kan inte detekteras för sig, utan partiklarna kommer att skapa så kallade jets som man sedan kan analysera. Vid många av experimenten som görs vid LHC, så kolliderar man tunga bly- eller guld-joner med väldigt hög energi. Detta kan skapa ett tillstånd som är så hett och så tätt så att kvarkarna och gluonerna kommer att bete sig som fria partiklar. Detta tillstånd kallas för kvark-gluon plasma och är ett tillstånd som existerade bara några microsekunder efter Big Bang. De energirika partiklarna kommer att skicka ut strålning i form av gluoner, på ett liknande sätt som elektroner under acceleration skickar ut fotoner. Detta sker både innan kollisionen och efter kollisionen.

I detta projektarbete så kommer det att undersökas hur jets blir påverkade av gluon-strålning som skickats ut innan en partikel kollision (även kallad för ISR (initial state radiation)). Detta kommer göras genom att undersöka till vilken utsträckning som jet energin och jet-rörelsemängd ändras beroende på ISR. Detta görs för både proton-proton kollisioner och för kollisioner med blyjoner.

Contents

List of acronyms

SM- Standard Model
QCD- Quantum Chromodynamics
pQCD- Perturbative Quantum Chromodynamics
LQCD- Lattice Quantum Chromodynamics
QGP- Quantum Gluon-plasma
LHC- Large Hadron Collider
RHIC- Relativistic Heavy Ion Collider
ISR- Initial State Radiation
FSR- Final State Radiation
HIC- Heavy-Ion Collisions
PDF- Partonic Distribution Function
MC- Monte Carlo
COM/CM- Center-of-mass
wrec - With recoiling particles
worec - Without recoiling particles

1 Introduction

Ever since the ancient Greeks coined the concept of the atom, physicists have been in a constant endeavour to find the smallest constituents of the universe. The contemporary efforts can be embodied, more or less, into a single model of theoretical physics, the Standard Model (SM). The Standard Model is a quantum field theory, which describes what kind of particles exist at a fundamental level and how they interact with each other. Just like it was discovered by Thomas Rutherford and James Chadwick that the atoms contain a collection of particles, i.e. electrons, protons and neutrons, recent efforts, done in the '60s and the '70s [1], showed that protons and neutrons are made up of even smaller particles, quarks, which are bound together by strong interaction. At the moment, quarks are considered to be fundamental in the SM and there are no experiments suggesting otherwise. In the SM, there are three types of fundamental particles, which are categorized depending on their spin quantum number. There are the fermions, which are half-integer spin particles and make up all the observable matter in the universe. These can be further categorized into quarks and leptons. Then there are the gauge bosons which have a spin of 1 (or -1) and act as force carriers. These are the particles that give rise to all the interactions between the other particles, e.g. the gluons give rise to strong interactions. Lastly there are the scalar bosons whose spin is zero. In the SM there exists only one scalar boson, namely the Higgs boson. This particle generates mass through its interaction with other fundamental particles through a process that is known as the Higgs mechanism.

The quarks and the gluons are of special interest to theoretical physicists because they can interact with the strong force. This is because they have a color charge, which acts like electrical charge for electromagnetic interaction. The strong interaction between quarks and gluons is described by the theory known as quantum chromodynamics (QCD), which has the symmetry group SU(3). This symmetry group gives rise to something known as colour confinement and asymptotic freedom. Colour confinement essentially means that, normally, no colour-charged particle can exist in a free state. Quarks and gluons can only exist bound together in color-neutral states known as hadrons. There are two types of hadrons, baryons and mesons. The baryons consist of an odd number of valence quarks (at least 3), but baryons with more than three valence quarks are extremely unstable and hard to detect. The mesons consist of an equal number of valence quarks and valence anti-quarks, but the most stable ones only have one of each. This means that experimentally, quarks can never be seen directly. Instead, quarks and gluons are observed indirectly through the formation of jets in experiments. A jet is a narrow cone-like collection of hadrons or mesons, travelling in the same direction, that are produced by colliding hadrons or ions at high energies. For a while, hadrons were believed to be the only states for quarks but in 1974, a paper was released with the suggestion of a new state of matter [2]. This state would be an extremely dense state of quarks and gluons where the particles no longer had to be confined into baryons or mesons. At this state, chiral symmetry, which normally is spontaneously broken, would be restored. We know from lattice calculations and experiments that in this state, the quarks and gluons would still be strongly interacting (albeit the interaction strength would reduce) and showing collective behaviour. They would behave like a relativistic hydrodynamic fluid with an extremely low shear viscosity. This state would later be called quark-gluon plasma (QGP) and is attainable by, for instance, colliding heavy ions at extremely high energies [3]. The conditions in this state are comparable to the quark epoch of the early universe, at a time estimated to be around one millionth of a second after the Big Bang [4]. Experiments like ALICE, ATLAS and CMS at CERN's Large Hadron Collider (LHC) have studied QGP in an attempt to recreate and understand the early stages of the universe, where QGP was dominant. With the LHC hitting a record breaking 5.02 TeV center of mass energy, the experiments seem very promising in finding exciting results. These

experiments investigate the properties of the QGP, e.g. at what temperature it is formed, how density affects the phase boundary, how it differs with baryon chemical potential. These experimens can impact fields like high energy physics, nuclear physics, cosmology, hydrodynamics and etc. These experiments might also shed light upon the origin of matter and mass [5]

1.1 Aim of the Thesis

When colliding heavy-ions at high energies, the first processes to occur are hard scattering processes that produce energetic partons. These processes have large momentum transfer and correspond to short time scales. The produced partons will then traverse the QGP state that is created due to the very dense state after the collision and develop into jets that we see in the detector. The structure of the jets depend mainly on the parton distributions of the colliding hadrons and on the matrix elements. Due to the extremely dense medium, the jets will interact strongly with the medium through elastic and inelastic scattering and lose energy, and this is called jet quenching. Jet quenching is one of the more prevalent methods of determining if a QGP state has been reached. So the jets traversing the medium, will interact with the medium with soft and semi-soft interactions, exciting constituents of the medium, which will then propagate with the jets affecting some of the jet quenching observables. This effect is called medium response. At the hard scattering processes, the highly energetic quarks and gluons that are scattered will radiate out gluons, similar to bremsstrahlung in electrodynamics where electrically charged particles emit photons when accelerated or decelerated. These gluons are primarily radiated in two directions in space. Before the hard-scattering processes, the partons will send out initial state radiation, relatively parallel to the beam axis, and after the hard-scattering processes, the produced particles will emit final state radiation radiation. Thus the initial state radiation will be mostly radiated along the original beam direction, whereas the final state radiation will be radiated mostly along the direction of the scattered particles. After the collision has then occurred, creating an hydrodynamic expansion and then producing a large number of hadrons, these hadrons can then cluster together with the initial state radiation, resulting in the jets having a fraction of the energy and momenta coming from the initial state radiation.

The aim of this thesis is to see to what extent, initial state radiation will affect the energy and momenta and the internal structure of the jets. Observables like jet production cross section, energy and momentum will be investigated for different starting parameters, e.g. jet radius, intensity of initial state radiation, number of colliding particles etc. This will be done for both proton-proton and heavy-ion collisions, where in the latter system, the role of jet quenching will be investigated. Further, in the case of the heavy-ion collisions, this thesis will investigate to what extent initial state radiation can be disentangled from the medium response.

1.2 Structure of the Thesis

In section 2, relevant theory is explained that is needed to interpret the results. In particular Quantum Chromodynamics, Quark-gluon Plasma, Jets and Heavy-Ion collisions are explained, since these are the primary topics of the thesis.
In section 3, the analyses of the thesis are explained. Here, the software that will be used will be explained and the parameters and observables of the analyses will also be discussed.
Section 4 the results obtained are presented with small jets first ($R = 0.3$) and later big jets ($R = 1.0$). These are sorted by beam-energy and JEWEL version (c.f. section 2.4.1).
Finally in section 5 all the conclusions are presented and at the very end, possible improvements are also discussed.

2 Theory background

2.1 Quantum Chromodynamics

Quantum Chromodynamics (QCD) is a quantum field theory, which describes how particles with the quantum number colour interact with each other through the strong interaction. In QCD, there are three colour charges and three respective anticolour charges, namely red (r), blue (b) and green (g) and antired ($\bar{r}$), antiblue ($\bar{b}$) and antigreen ($\bar{g}$). In the SM, only the quarks and the gluons carry colour charge. QCD is a non-abelian gauge theory with symmetry group SU(3). The gauge invariant Lagrangian of QCD, that describes the interactions between quarks and gluons is:

$$\begin{aligned} \mathcal{L}_{QCD} &= \overline{\psi}_i(i(\gamma^\mu D_\mu)_{ij} - m\delta_{ij})\psi_j - \frac{1}{4}G^a_{\mu\nu}G^{\mu\nu}_a \\ G^a_{\mu\nu} = \partial_\mu A^a_\nu - \partial_\nu A^a_\mu + g f^{abc} A^b_\mu A^c_\nu, &\qquad D_\mu = \partial_\mu - ig\lambda_a A^a_\mu \end{aligned} \tag{2.1}$$

Where ψ is the quark field, γ^μ are the Dirac matrices, $G^a_{\mu\nu}$ is the gauge invariant gluon field strength tensor, A^a_μ are the gluon fields, D_μ is the covariant derivative, g is the coupling strength of the interaction and λ_a are the Gell-Mann matrices.
Because of the cubic and quartic powers arising from the interactions of the gluon field, the Lagrangian is impossible to solve analytically and must instead be solved with either perturbation theory (pQCD), i.e. with approximate solutions, or numerically with Lattice QCD (LQCD). pQCD only works for high-energy or short-distance interactions. In pQCD, approximate solutions are obtained through finite power series, where the variational method can be used if the series are divergent. Perturbative QCD is not valid for low energies, since the coupling strength α_s becomes too large, making the perturbations too large for perturbation theory to be valid. LQCD is a numerical approach to solving QCD. It is a lattice gauge theory, which works by placing the quarks on the lattices and the gluon fields as the connecting lines between the lattice points [6]. If the latice spacing is finite then the formulation is a discrete formulation. But as the lattice becomes infinitely large and the lattice separations become infinitely small, LQCD will properly describe a continous spacetime. It is valid to use LQCD, in contrast to pQCD, in low-energy scales.

The gluons are in the adjoint representation of the $\mathrm{SU}(3)_C$ gauge symmetry, which means that the gluons transform non-trivially under a gauge transformation, leading to the gluons themselves having colour. The quarks carry one of the three types of colour charge whereas the gluons carry both a colour and an anticolour charge. There exist eight independent color states which the gluons can have, called a gluon octet, and these correspond to eight different types of gluons. These states can be represented as:

$$\begin{aligned} (r\bar{b} + b\bar{r})/\sqrt{2}, &\qquad -i(r\bar{b} - b\bar{r})/\sqrt{2} \\ (r\bar{g} + g\bar{r})/\sqrt{2}, &\qquad -i(r\bar{g} - g\bar{r})/\sqrt{2} \\ (b\bar{g} + g\bar{b})/\sqrt{2}, &\qquad -i(b\bar{g} - g\bar{b})/\sqrt{2} \\ (r\bar{r} + b\bar{b})/\sqrt{2}, &\quad -i(r\bar{r} + b\bar{b} - 2g\bar{g})/\sqrt{6} \end{aligned}$$

These are the eight independent states that a gluon can have that are superpositions of the colour combinations: $r\bar{b}, b\bar{r}, r\bar{g}, g\bar{r}, b\bar{g}, g\bar{b}, r\bar{r}, b\bar{b}$ and $g\bar{g}$. Since gluons carry colour they can self-interact. This leads to interesting phenomena like color confinement and asymptotic freedom.

2.1.1 Strong Coupling Constant and Asymptotic Freedom

Due to the gluons being able to interact with each other, the higher order corrections will include gluon loops that effectively have an antiscreening effect that decreases for higher energies, since the probability of emitting gluon radiation increases, meaning that there will be less gluons to antiscreen the quark. The effect of the antiscreening is that the net colour of a quark observed by a probe is increased. There also exist quark loops which have a screening effect, but this is smaller than the loop contributions from the gluons due to there being more gluons. This means that the coupling constant is not constant, but rather depends on the energy scales, the distance or the momentum transfers in the interaction. The running of the coupling constant is described by:

$$\mu^2 \frac{\mathrm{d}\alpha_s}{\mathrm{d}\mu^2} = \beta(\alpha_s) \tag{2.2}$$

Where μ is the energy-scale or momentum transfer and β is the beta-function. In pQCD,

$$\beta(\alpha_s) = -\alpha_s^2 \left(\beta_0 + \beta_1 \alpha_s + \beta_2 \alpha_s^2 + ...\right)$$

where β_0, β_1, β_2, correspond to one loop correction, two loop- and three loop corrections respectively.
Since $\beta(\alpha_s)$ is negative, the solution to the differential equation 2.2 is for the one loop aproximation (i.e. keeping only β_0) [7]:

$$\alpha_s(\mu^2) = \frac{\alpha_s(\mu_0^2)}{1 + \beta_0 \alpha_s(\mu_0^2) \ln(\mu^2/\mu_0^2)} = \alpha_s(\mu_0^2) \sum_{n=0}^{\infty} \left(-\beta_0 \alpha_s(\mu_0^2) \ln \frac{\mu^2}{\mu_0^2}\right)^n$$

Setting $\Lambda^2 = \mu_0^2 \exp\left(-\frac{1}{\beta_0} \frac{1}{\alpha_s(\mu_0^2)}\right)$, allows for $\alpha_s(\mu^2)$ to be written with the scale Λ:

$$\alpha_s(\mu^2) = \frac{1}{\beta_0 \ln(\mu^2/\Lambda^2)} \tag{2.3}$$

For n_f flavour of quarks:

$$\beta_0 = \frac{11 - \frac{2}{3} n_f}{4\pi}$$

Equation 2.3, clearly shows that the coupling constant decreases logarithmically, which means that at high energies, the interaction strengths will become much weaker. This effect is known as asymptotic freedom.

2.1.2 Colour Confinement

Colour confinement is a property of QCD that states that quarks and gluons can not be in a non-colour neutral state. The quarks and gluons must be in colour neutral states like baryons, mesons or the theoreticized states, glueballs, which consists of three or more valence gluons and virtual gluons and quarks (there is controversy in whether or not this state has been observed experimentally, see e.g. [8], [9]). Similarly, the hadrons contain valence quarks instead and a sea of virtual quarks and gluons. These virtual gluons will interact softly within the color neutral state, binding the color neutral state more. The field energy inside a color neutral state, e.g. a meson can be explained with flux tubes. If the valence partons in the mesons interact with e.g. a gluon, resulting into energy being transferred to the parton, the two partons will separate. Because of the gluon self-coupling, the cross-sectional area of the tube will remain almost constant for all separation between the valence quarks, but the larger the separation,

the more soft gluon interactions there will be. This means that the energy stored in the gluon field increases as well. As the separation increases, at some point the energy will be high enough to create a real particle pair. Then it would be energetically favourable to create the two partons, where the newly formed parton pair forms two new colour neutral state with the original partons. This is depicted in figure 1.

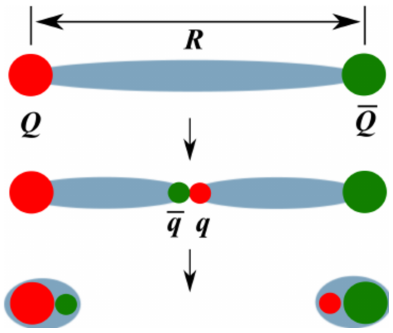

Figure 1: A schematic figure depicting a production of a meson pair. As the distance, R, between the two original partons increase, so does the energy. Image taken from: [10]

2.1.3 Chiral Symmetry

Chiral symmetry is the invariance of the QCD Lagrangian under an axial flavour transformation. In the infinitesimal form, the axial flavor transformation is:

$$\delta\psi_i = -i\delta\alpha^a (T^a)_i{}^j \gamma_5 \psi_j, \quad \delta\bar{\psi}_i = -i\delta\alpha^a \bar{\psi}_j \gamma_5 (T^a)_j{}^i$$

where α is a phase, T^a are $n_f \times n_f$ hermitian traceless matrices, and n_f is the number of flavours. The QCD Lagrangian will not be invariant during an axial flavour transformation, because of the mass terms for the quark. Thus a true chiral symmetry, requires the vanishing of the quark mass terms. In nature, quarks do have masses, which means that chiral symmetry is not an exact symmetry for QCD. This means that the particles transform differently depending on their parity. This is known as explicit chiral symmetry breaking. If the ground state, i.e. the vacuum state, is not invariant under a chiral transformation, then the chiral symmetry is spontaneously broken. This leads to mass generation in the baryons. This is because the QCD binding energy arises when the chiral symmetry is spontaneously broken. This mass generation accounts for 99 % of the visible mass in the universe.

2.1.4 Quark-gluon Plasma

Quark-gluon Plasma (QGP) is a state of matter, at which either the baryon density is significantly higher than the normal nuclear matter density and/or the temperatures are higher than a critical value, T_c. The STAR Collaboration at the Relativistic Heavy Ion Collider (RHIC) at Brookhaven National Laboratory, has defined the QGP as: "*a locally thermally equilibrated state of matter in which quarks and gluons are deconfined from hadrons, so that color degrees of freedom become manifest over nuclear, rather than merely nucleonic, volumes* " [11].

However, even though the particles are deconfined, experiments have shown that the quarks and the gluons are still strongly interacting, albeit the interaction strength is expected to become weaker with increasing temperature. The QGP created in heavy-ion collisions can be described by relativistic hydrodynamics, except at the early and late stages of the collision, i.e. at the crossover stages, where there is no local thermal equilibration.

The phase transition is illustrated in figure 2, which is a schematic figure of the QCD phase diagram, with the parameters temperature, T, and baryon chemical potential, μ_B, which is a measurement of the excess of quarks over anti-quarks. μ_B is directly related to the baryon number at central rapidity and to the energy of the collision. This means that it can be adjusted by changing the beam energies. If $\mu_B = 0$, this means that there is a perfect balance.
The precise location of the phase transition is not known, neither experimentally nor analytically, and numerical solutions through lattice QCD can only be made for vanishing values of the baryon chemical potential, i.e. $\mu_B \simeq 0$. The crossover temperature is found by looking at the number of degrees of freedoms in the hadron gas and the number of degrees of freedom in the QGP. At the phase-transition from the hadronic gas to the QGP, a rapid increase in pressure is expected since the increase in the number of degrees of freedom will lead to an increase in entropy. Numerical estimations through LQCD (c.f. figure 3), predicts crossover transition at $T_c \sim 150 - 170$ MeV [13]. At very small values for the baryon chemical potential, i.e. $\mu_B \approx 0$, there is no phase transition. Coincidentally, numerical simulations through lattice QCD have shown that for low baryon chemical potential, there will be a chiral symmetry restoration at approximately the same temperature as the crossover transition to the deconfined phase. The exact reason for why the transition temperature for the chiral symmetry restoration, T_χ and the deconfinement, T_c, occurs at the same temperature is not known.

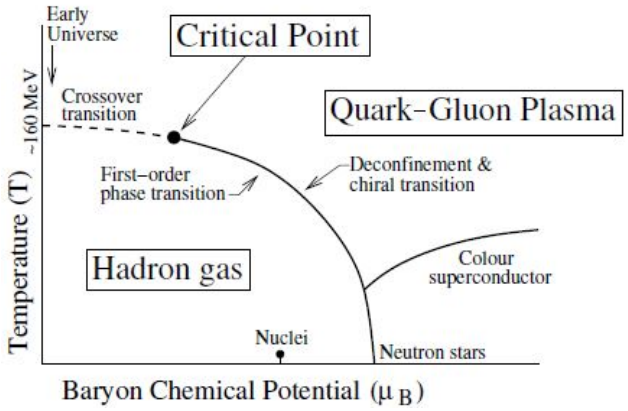

(a) Figure 2. A schematic QCD Phase diagram showing how the phase transitions may look for different values of baryon chemical potential and temperature. Figure taken from [12].

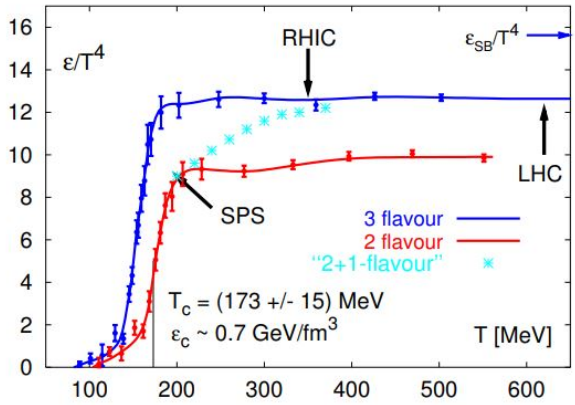

(b) Figure 3. A plot of the energy density (which in a fluid is considered equal to the pressure) on the y-axis as a function of the temperature on the x-axis with $\mu_b = 0$. This is performed with LQCD for massless quarks. A crossover temperature can be seen due to the sudden increase in pressure or energy density. Image taken from [13].

2.2 Jets

When performing experiments with high-energy particle collisions, the partons can not be observed directly due to color confinement. The partons will fragment into collimated sprays of hadrons, that can then be observed by the detectors. Due to momentum conservation, these will end up in a narrow conical shape in the same direction, where the collection of the particles is conceptually defined as a jet. This definition, however, doesn't allow for any useful information to be extracted. Due to the quantum mechanical nature, it is impossible to make conclusions on the interactions by analysing each hadron individually. Therefore, jets are a very important theoretical tool to determine what kind of physical processes are occuring. Relevant information can be extracted by collecting data from the collection of hadrons produced, i.e. the jets produced. To be able to extract relevant information from jets, it's necessary to have

a proper definition for jets. There is no unique definition, but a proper jet definition needs to have a jet algorithm, which determines which of the particles belong to what jet based on some parameters and it needs to have a recombination scheme, which is a way of recombining the particles' four-momenta. Some algorithms recombine particles into one particle, i.e. a pseudojet, to mimic the QCD dynamics that happen in the parton shower and will trace back events to the partons coming from the initial hard scattering event. Besides that, there are some important criteria a jet definition has to fulfil to be considered a good definition [14]:

(i) A good jet definition should be easy to implement in an experimental analysis and in a theoretical calculation.

(ii) A good jet definition should be defined at any order of perturbation theory.

(iii) A good jet definition should give finite cross sections for any order of perturbation theory, that are relatively insensitive to hadronisation.

2.2.1 Infrared and Collinear Safety

A good jet algorithm must be infrared and collinear (IRC) safe in order to compare experimental results to fixed order perturbative QCD, as otherwise there would be divergences that do not cancel, leading to infinite cross sections. An observable is infrared safe if it is invariant to the emission of infinitely soft particles, i.e. zero energy gluons. An observable is collinear safe if it is invariant to collinear splitting, i.e. the splitting of a particle into two co-moving particles. IRC safety essentially covers point (ii) and (iii) in the previous paragraph. So in an IRC safe jet algorithm, collinear splitting and infrared radiation can not affect the hard jets. Infrared and collinear safety is also needed so that real-virtual cancellation are not lost in next-to-leading order and next-to-next-to-leading order QCD calculations. Further, the detector is unable to resolve infrared or collinear event structures.

2.2.2 Kinematic Variables

In collision experiments, the four-momentum of a particle $p^\mu = (E, p_x, p_y, p_z)$ is more naturally written with the quantities, transverse mass m_t (or m_δ), transverse momentum p_T, rapidity y and azimuthal angle θ. In natural units, i.e. $c = \hbar = 1$, these quantities are defined as

$$\text{Transverse mass: } m_t = \sqrt{m^2 + p_T^2}$$
$$\text{Transverse momentum: } p_T = \sqrt{p_x^2 + p_y^2}$$
$$\text{Rapidity: } y = \frac{1}{2} \ln \frac{E + p_z}{E - p_z}$$

where p_z is the momentum-component along the beam direction. The four-momentum can then be written as:

$$p^\mu = (\,(m_\delta + p_T)\cosh(y),\, p_T \cos(\theta),\, p_T \sin(\theta),\, (m_\delta + p_T)\sinh(y)\,) \tag{2.4}$$

where $m_\delta = m_t - p_T$.
These are more convenient since the transverse mass and the transverse momentum are scalars and the rapidity has a simple transformation under a Lorentz transformation along the beam axis. With these variables, the distance between two particles i and j in the (y, θ) plane is:

$$R_{ij} = \sqrt{\Delta y_{ij}^2 + \Delta\theta_{ij}^2} \tag{2.5}$$

The energy in particle collisions are often expressed in terms of nucleon-nucleon COM energy, $\sqrt{s_{NN}}$, or the total COM energy, $\sqrt{s}$. The relation between these are:

$$\sqrt{s} = A\sqrt{s_{NN}} \tag{2.6}$$

where A is the number of nucleons in each nuclei.

2.2.3 Formation of Jets

The production of jets involves a series of processes and is different in e.g. e^+e^- collisions and pp collisions. Since protons are composite objects, this will be far more complicated than e^+e^- collisions, and ion-ion collisions will be even more complicated.

In pp collisions, when the colliding protons are extremely close, i.e. at length scales at $\sim$ 1 fm, the overlap of the wavefunctions of the two partons will start to matter, increasing the probability of a hard scattering. During the collisions, the first processes that occur are the hard-scattering processes with large momentum transfer Q, where partons from each proton interacts with each other, creating new gluons or quarks. The incoming partons can emit radiation in the form of gluons, so-called initial state radiation (ISR). This radiation is highly reminiscent of bremsstrahlung in quantum electrodynamics, where accelerated charged particles emit photons. The likelihood of hard scattering happening is determined by the cross section of the process:

$$\sigma(P_1, P_2) = \sum_{i,j} \int_0^1 \mathrm{d}x_1 \mathrm{d}x_2 f_i(x_1, Q^2) f_j(x_2, Q^2) \hat{\sigma}_{ij}(x_1 P_1, x_2 P_2, \alpha_s, Q^2)$$

where P_1, P_2 is the 4-momentum of the two protons, x_1, x_2 is the fraction of the proton momentum the parton carries, $f_i(x, Q)$ are the parton distribution functions (PDF) and $\hat{\sigma}_{ij}$ are the partonic cross sections. The newly produced parton(s) will then be travelling away from the interaction point with a transverse momentum that depends on the partonic cross section. Because of large differences in the energy scales of the hard processes and the scale of hadronisation, the collinear enhanced processes, i.e. gluon radiation, will fill the phase space. This allows for the hard partons to radiate a lot of gluons or quarks and this radiation, and all other radiation that comes after the hard scattering processes, are called final state radiation (FSR). The partons in the protons can also interact through soft-scattering processes, which means that the momentum transfers are low. Lastly, the original protons will have beam remnants that interacted with other partons, and will thus hadronize into hadrons with momentum along the original beam axis. Different processes are shown in figure 3. It is impossible to experimentally differentiate, on a jet-by-jet basis, between ISR/FSR/soft-scattering processes and the beam remnants that make up the jet.

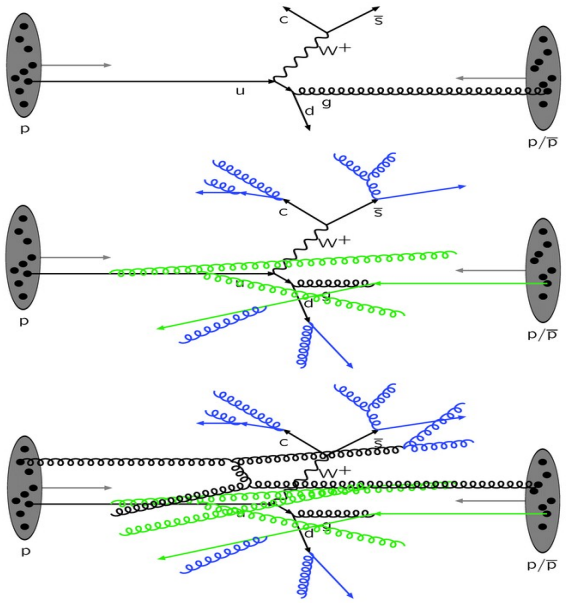

Figure 3: Image showing three types of processes in pp collisions. Black lines represent hard scattering processes, green lines represent ISR and blue lines represent FSR. Figure taken from [15].

2.2.4 Jet Algorithm

The jet algorithms are typically divided into two classes, namely cone algorithms and sequential recombination algorithms. The (well defined) jet algorithms have different strengths and weaknesses, e.g. the cone algorithms are generally infrared and collinear (IRC) unsafe (except the SIScone algorithm [16],) but are easier to implement. The cone algorithms assume that particles will appear in conical regions and therefore cluster the particles based on $(y-\theta)$ space and are used e.g. at the Tevatron [16]. Some examples of cone algorithms are FC-PR,IC-PR, IC-SM and SIScone.
The sequential recombination algorithms are the more popular algorithms as of today due to a number of reasons. Most importantly, they are all IRC safe [17]. In the past the sequential recombination algorithms were much slower than the cone algorithms and the computation time scaled as $\mathcal{O}(N^3)$, where N is the number of particles. But with the FastJet algorithm, it performs a lot faster and scales as $\mathcal{O}(NlnN)$ [18], making it faster than the cone algorithms. All the sequential recombination algorithms work backward, in the sense that they look at the end of an event and pair particles into a single entity based on their distance and momentum difference. There are two distance variables used in sequential recombination algorithm. The distance variable d_{ij} between two particles i and j and the distance variable d_{iB}, which is the difference in momentum between particle i and the beam. They are defined as:

$$\begin{aligned} d_{ij} &= \min(p_{T_i}^{2p}, p_{T_j}^{2p})\frac{R_{ij}^2}{R}, \\ d_{iB} &= p_{T_i}^{2p} \end{aligned} \tag{2.7}$$

where $2p$ is an exponent that determines the type of algorithm, R_{ij} is the distance in the (y,θ) plane as defined in equation 2.5, and R is the radius parameter which determines how big a jet will be.

The algorithm works by finding the smallest value in the set $\{d_{ij}, d_{iB}\}$ and combining the two particles i and j into one particle by summing the four-momenta. The original particles are then removed from the set. If the minimum is d_{iB} then i is proclaimed as a jet. Particles

that are bunched up with jets simply add their four momenta to the jet. This is then repeated until all the particles are assigned to a jet.

Some examples of sequential recombination algorithms are k_t (with $p = 1$), $Anti - k_t$ (with $p = -1$) and Cambridge/Aachen (with $p = 0$). In this project only the $Anti - k_t$ will be used, meaning that:

$$\begin{aligned} d_{ij} &= \min\left(\frac{1}{p_{T_i}^2}, \frac{1}{p_{T_j}^2}\right)\frac{R_{ij}^2}{R} \\ d_{iB} &= \frac{1}{p_{T_i}^2} \end{aligned} \tag{2.8}$$

As is seen in equation 2.8, the d_{ij} will be small for high p_T and will thus in general cluster hard particles first. This leads to regular shaped circular jets for which it is easier to apply corrections for underlying event processes. The $anti - k_t$ algorithm is very good in resolving jets but is worse than the other sequential recombination algorithms when it comes to investigating the jet substructure. When reconstructing the jet, contributions from ISR, FSR and soft underlying events (together they are called multiple-particle interactions), can end up in the jet if they are close in phase-space to the original hard partons. Contributions to the jet, from other sources than the main contribution, are corrections to the "jet = parton" picture that is used in the jet algorithms.

2.3 Heavy Ion Collisions

The processes that occur in heavy-ion collisions (HIC) are similar to the ones in *pp*-collisions, except that there are a lot more interactions. Compared to *pp*-collisions, if the beam is accelerated in the same accelerator with the same machine settings, the energy per nucleon will be smaller in HIC by a factor of $\frac{Z}{A}$, where Z is the number of protons and A is the number of nucleons. However, since there are a significant amount of nucleons in a dense state, there will be a lot more interactions and this creates a large energy density ($\sim$ 12 - 14 GeV/fm^3 for central $Pb - Pb$ collisions at $\sqrt{s_{NN}} = 2.76$ TeV [25]) over a large volume ($\sim$ 5000 fm^3). With high-energy HIC, it is thus easier to produce a QGP state and explore the properties of the QGP state. The evolution of a HIC at collider energies can be explained by five stages.

2.3.1 Initial State

The conditions of the heavy-ions and the nucleons of the ions just before and just during the collision, is regarded as the initial state of the collision. At this state, properties like e.g. beam energy, number of collisions, N_{coll}, the number of participant nucleons, N_{part}, and the geometry of the collision of the heavy ions play a determining role in the creation of the jets that are later observed. Due to the extremely large energies of the ions, at the centre-of-mass frame the two ions will be Lorentz contracted longitudinally and can be pictured as two thin disks colliding (c.f. figure 4). In JEWEL (c.f. 2.4.1), which uses a simple Glauber model, the only thing needed to determine the number of collisions and participants is the impact parameter b, i.e. the transverse distance between the centres of the two colliding ions, the nucleon-nucleon cross section (which is a function of $\sqrt{s_{NN}}$) and the geometry of the collisions. If b is small then the collision will be very central and more particles will be produced in the collision. The impact parameter is however not accessible through experimental measurements and thus instead the centrality, which is the geometric cross section, is used to classify the initial state geometry of HIC. In experiments, centrality ranges are determined by looking at the particle multiplicity at the final stage.

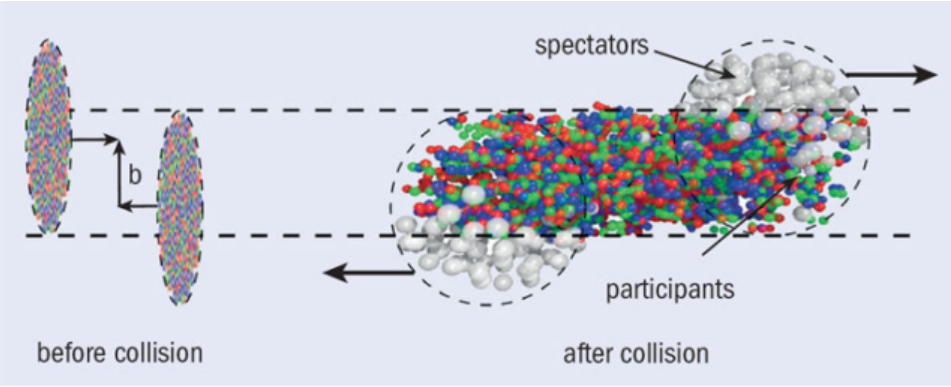

Figure 4: A figure depicting a collisions between two heavy ions that are Lorentz heavily contracted and have a distance b between the two centres. Image taken from [27].

Due to the very short range of the QCD interactions, the interactions will be fairly reduced in peripheral collisions, meaning that the total particle multiplicity is also reduced. This means that it in average is greatest for very central collisions. Typically, the centrality is measured by observing the charged particle multiplicity (since it's easier to detect) or by looking at the number of spectator nucleons, i.e. nucleons that did not interact in the collision, and try to fit a multiplicity distribution using the Glauber model [26].

2.3.2 Pre-equilibrium

This stage includes the collision, i.e. the overlap of the nuclei and the hard scattering processes. These take place at a time scale of about 0.1 - 1 fm after the collision. In this stage the hard processes occur, that can be described by pQCD. This stage is a stage where the systems expands very rapidly, so there is no equilibrium and hydrodynamic models can not be applied. However, due to the large momentum transfers, real (and virtual) photons can be produced that can give information about the momentum distribution of the system at this stage.

2.3.3 QGP, Expansion and Hadronization

After the systems size has increased, the particles that are produced from the collision will continue to interact and the system will become a QGP state at a time around 1 fm after the collision. After the QGP state has been created, the internal pressure will be extremely high, which will cause the system to expand rapidly, causing the energy density to decrease. This expansion is usually described by relativistic hydrodynamics [28]. At around 10 fm after the collision the energy density will reach the critical density, $\epsilon_c \sim 1$ GeV [28], at which the system is no longer in a QGP state ($\epsilon_c \sim 1$ GeV [28]). After it has reached the critical density the hadronization phase will begin, where quarks, anti-quarks and gluons will be bound into color neutral states. The hadrons will interact with each other through both elastic and inelastic processes and the system will continue to expand and cool.

2.3.4 Chemical and kinetical freeze-out

After 10 fm, as the system continues to cool, the density will be too low and the hadrons inside the system will not have enough energy to interact inelastically with each other and change hadron species. When this happens the system enters chemical freeze-out. It has been argued that the chemical freeze-out happens very close to the phase boundary [29]. At this stage, the hadrons are still close enough to each other to interact through collisions. When the density of the systems becomes too low, so that the hadrons are too far separated, the system enters kinetical freeze-out. The particles will not interact with anything else until they reach the detectors.

2.3.5 Jet Observables

Some of the more typical jet obervables in experiments are jet multiplicity, i.e. the number of jets that are produced, jet mass and jet p_T, jet charge, different jet spectras (for instance p_T, energy, rapidity or pseudo rapidity), jet-shape, cross section etc. Other important parameters in an HIC are the number of binary nucleon-nucleon collisions, N_{coll}, which is typically calculated using the Glauber model [22], the number of participant nucleons, N_{part}, which can be inferred by looking at the spectator nucleons and missing p_T.
The jet-shape $\rho(r)$ describes the average distribution of transverse momentum inside the jet [21]. It is defined as:

$$\rho(r) = \frac{1}{\delta r}\frac{1}{N_{\text{jet}}}\sum_{\text{jets}}\frac{\sum_{\text{tracks}\in|r_a,r_b)} p_T^{\text{track}}}{p_T^{\text{jet}}} \tag{2.9}$$

where the jet cone with jet radius R, is divided into $R/\delta r$ annuli with the width δr, and where each annulus has $r_a = r - \delta r/2$ and $r_b = r + \delta r/2$ as the inner and outer radius respectively. Here, r is the radial distance from the track to jet axis in (η, ϕ) space.
To calculate the ISR jet-shape, then the tracks in equation 2.9 are only from ISR particles.

2.3.6 Jet Quenching

When an AA collision produces a QPG state, the hard partons that traverse through the QGP medium will suffer differential energy loss due to multiple interactions with the medium. This effect is called **jet quenching** and is one of the telltale signatures of the QGP state. When a hard collision that produces two jets occurs at the edge of the QGP medium, it is possible that one of the jets will traverse through the medium and subsequently experience jet quenching (even having the possibility of becoming completely absorbed), whereas the other jet doesn't traverse through the medium at all, or at least far less. This is depicted in figure 5. This would then indicate that a QGP state has been produced by studying the number of correlated jets at different angular separations. Knowing how much energy is lost by a parton provides information about the thermodynamical and transport properties, e.g. viscosities, diffusion coefficients, etc., of the QGP state.
The energy loss of the hard partons that traverse the QGP can happen either through elastic collisions with other partons or through gluon radiation, similar to QED Bremsstrahlung. The radiative energy loss component is the more important aspect of the two when it comes to jet quenching, as it is responsible for most of the energy loss [23]. The hard parton will radiate soft gluons at a frequent rate, that subsequently interact further with the medium. The rate and the energy transfer depends on the density of the QGP state, the energy of the hard parton and the cross section of the gluon-medium interaction. To determine how the jet quenching have affected the jet substructure, the jets are compared to similar collisions where a QGP state has not been formed. This can be done by comparing heavy-ion collisions with *pp* collision by for instance looking at the jet shapes produced.
The jet shape nuclear modification factor is defined as the ratio of the jet shape between heavy-ion collisions and *pp* collisions at different distances r. For an unquenched jet, this value would simply be 1, whereas a quenched jet would have a value less than 1. If it is higher than 1, then it means that the p_T contribution has been boosted in the region observed. This makes it possible to see how the jet is modified at different r.

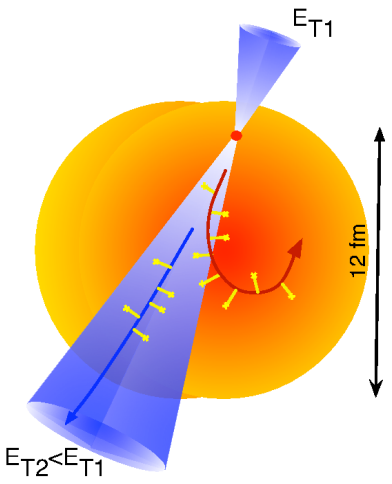

Figure 5: A figure depicting two jets where the seed partons are created near the boundary of the QGP state (orange region). Picture taken from [20].

In JEWEL (c.f. section 2.4.1), jet quenching is handled by first providing a solid model of the interactions with the medium. The medium is treated as a collection of partons that act as scattering centres. JEWEL then simulates the hard parton's propagation through the medium, where it undergoes several scattering processes (as depicted in figure 7). The scattering probability is determined by the path length inside the medium, the density- and the cross section of the thermal particles.

2.3.7 Medium Response

As the hard partons traverse the medium, radiating gluons all the way, the lost energy of the hard partons will be deposited into the medium. If the energies are high enough, this would mean that particles in the medium would now have a measurable momentum in the jet direction and these particles may then hadronize, becoming a part of the jet. While the additional soft activity due to medium response may affect some of the jet observables, e.g. the anisotropic flow pattern of the bulk matter [24]. Due to momentum conservation, the particles that are created from the medium response will be moving along the jet and thus the bigger the jet radius is, the larger the part of the energy that is recovered will be. Since the particles due to medium response are distributed over very large angles, it will however be impossible to recover everything inside the jet. The background that is created from the medium response can not be subtracted from the jet since at hadron level, it is impossible to assign a certain hadron to the jet or medium response. Instead, the additional soft particles that come from the medium response must be treated as a part of the jet.

2.4 Software used

Rivet [34] is an analysis toolkit that performs an event-per-event analysis on high-energy-physics-monte-carlo (hepmc) events. Rivet is the most wide-spread method of using analysis code from the LHC and other HEP experiments to compare with future theory models. FastJet [33] is a C++ package that is used to cluster particles into jets based on the jet algorithm used. It can also manipulate the jet substructure if that option is desired.

2.4.1 JEWEL

JEWEL [30] is a Monte Carlo (MC) event generator that simulates QCD jet evolution in heavy-ion collisions and pp collisions. JEWEL is also a physics model that specifies dynamically the relation between parton energy loss, p_T-broadening, recoil momentum, change in jet multiplicity and other features of parton energy loss. Monte Carlo event generators are by far the most used tool to describe jets in a multiple-particle system. This is because they are the best tool to compare a partonic evolution to the final state particles detected in an experiment. JEWEL, as compared to most other MC, simulates jet evolution in a medium, which allows for simulations of the jet-medium interactions that take place in the QGP state that is produced from relativistic HIC. The event generation follows three stages.
First the hard scattering processes that produce the di-jets and the corresponding initial state parton shower is generated through a modified version of PYTHIA 6.4 [31], which is another MC event generator. The particle distribution functions are provided by the LHAPDF library [32] and in this project the EPS 09 set will be used. After this, JEWEL determines the impact parameter b (based on input) of the collisions. Based on the number N_{coll}, it then simulates the final state parton shower, where the medium-interactions are included. The partons in the jet may interact with the thermal particles through $2 \rightarrow 2$ scattering processes, which are determined by the matrix elements. At the last stage, JEWEL again uses PYTHIA for the hadronisation, where the Lund string model is used [35][36].

JEWEL has three options to deal with medium response. Either it is ignored, or a source term can be extracted for hydrodynamic treatment or the third option is to keep the thermal partons from the medium that interact with the jet and let them hadronise together with the jet. The interactions with the medium is shown in figure 6. A particle in the medium with momentum p_{the} interacts with a parton produced from the hard scattering process. The gluon in the medium will then have momentum $p_{rec} = p_{the} + q$. JEWEL treats the medium as an ideal quark-gluon gas, which means that the momentum distribution is a Bose-Einstein or Fermi-Dirac distribution that is entirely determined by the temperature T of the QGP medium. The temperature is determined by looking at the energy density profile which in JEWEL is directly proportional to N_{part}. For this project, a modified version of JEWEL is used to distinguish between ISR partons from FSR partons. This version was provided by the creator of JEWEL, Korinna C. Zapp. When generating events with JEWEL-230, the partons from ISR will not interact with the medium, whereas with JEWEL-240 they will.

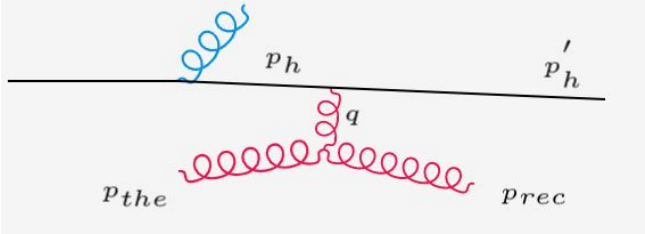

Figure 6: A figure depicting a parton interacting with the medium (red). The blue gluon is a FSR.

3 Analysis

3.1 Eventfile Generation

In this thesis, the impact of the ISR on the jet internal structure is studied for a numerous set of events. The events are generated with the MC event generator JEWEL. Eventfiles, containing 10^6 events, are generated for simulations in vacuum, corresponding to pp collisions,

and eventfiles containing 10^5 events, for collisions in a simple medium, corresponding to *PbPb* collisions. This is done for two center-of-mass energies; $\sqrt{s_{NN}} = 2.76$ TeV and $\sqrt{s_{NN}} = 5.02$ TeV. The *pp* collisions will serve as a reference to the more complicated *PbPb* collisions. To understand the impact of the medium response, and how it can be disentangled from the ISR contribution, eventfiles will be generated with both JEWEL-230 and JEWEL-240. For the partonic distribution functions, LHAPDF 5.8.4 [32] will be used with the EPS 09 set.

3.2 Parameters and Observables

In all of the analyses, the anti-k_t algorithm will be used, with the jet radius parameter $R = 0.2$. The clustering of the jets will be done through FastJet (3.3.2) [33]. When reconstructing the jet, only jets which have $p_T \geq 100$ GeV, will be considered. After the clustering is done, in the analysis only jets which have $|\eta_{jet}| \leq 2.5$, will be considered, i.e. only mid-rapidity jets. When investigating the jet shape only the region $0.3 \leq |\eta_{jet}| \leq 2.5$ will be considered. The region, $|\eta_{jet}| \leq 0.3$ is not examined to avoid overlap between the signal jet region and the background cone. The investigation of the impact of ISR will be done by examining:

- The energy and momentum fraction that is carried by ISR in the jet, will be measured for different jet observables, like the p_T spectrum, the y spectrum.
- The jet profile for the total jet momentum and the momentum carried by ISR in the jet, and the ratio of these two jet profiles.

For $R = 0.3$, $\sqrt{s_{NN}} = 2.76$ TeV, all of these measurements on the *PbPb* collisions will be done for different values of the centrality in the ranges: 0-10 %, 30-50 % and 70-100%
The event-per-event analysis will be performed with Rivet (version 2.7.2b) [34], which uses a C++ framework for the analyses. Lastly, the plots will be produced with YODA (version 1.7.7), which also provides the histogram functionality that Rivet uses.

3.3 Medium Response

To include the medium response, the thermal particles' momenta can not be added by just adding the regular four-momenta, as it is done in the anti-k_t algorithm. The background coming from the thermal particles have to be subtracted using constituent subtraction. In this way, the p_T and m_δ, as defined in equation 2.4, are subtracted from the nearest particles so that mass squares are guaranteed to be positive. The larger p_T particles "absorbs" the lower p_T one. This is repeated for all the particles within a cut-off region, which in this analysis is chosen to be $R_{ij} \leq 1.0$. The exact algorithm can be found at [37] [38].

4 Results

Here, the results obtained from performing the analyses will be presented. First, the result from the *pp* collisions will be presented (green in figures) to act as a reference to the *PbPb* collisions. Then the results from the *PbPb* collisions will be presented, with both events containing medium response, which are denoted as wrec (with recoiling particles), and events without medium response, worec (without recoiling particles). For $R = 0.3$ different centralities will also be plotted. The ISR-p_T fraction, i.e. the average fraction of the jet-p_T carried by initial state radiation, is plotted for different jet-p_T and y in *pp* collisions. Further, the jet-shape and ISR-jet-shape is plotted for different values of r. The relevant parameters will be included in the title of the section and the caption of the figure. The data will be sorted primarily by the radius R of the jet algorithm. Secondarily it will be sorted by the nucleon-nucleon CM energy, $\sqrt{s_{NN}}$ and by the version of JEWEL used. For $R = 0.3$, different centralities will also be examined, whereas for $R = 1.0$ only 0-10 % centralities are examined.

4.1 Results for small jets (R= 0.3)

4.1.1 Results with $\sqrt{s_{NN}} = 2.76$ TeV & JEWEL-230

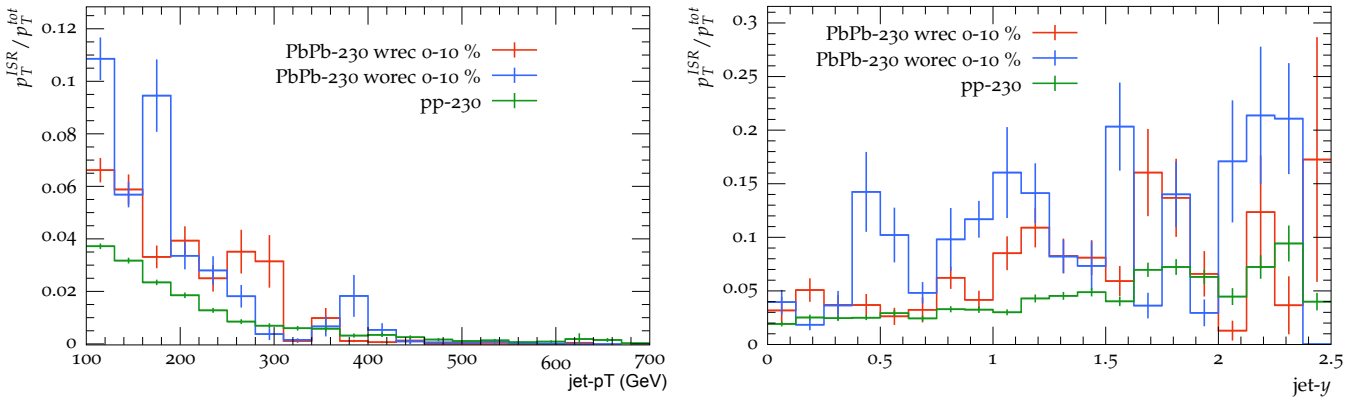

Figure 7: The ISR jet-p_T fraction is plotted for different jet-p_T and jet-y in pp-collisions (green) and in $PbPb$-collisions with JEWEL-230. HIC with medium response correspond to red lines, whereas without medium response correspond to blue lines. $\sqrt{s_{NN}} = 2.76$ TeV

In figure 7, it is seen that the p_T contribution is higher for the PbPb collisions with and without medium response. This is because in JEWEL-230, the ISR particles do not interact with the thermal particles in the QGP, meaning that the ISR particles will not be "quenched". It is also seen that the ISR p_T contribution is going down for increasing jet-p_T. This is expected since the initial state radiation, prior to the hard scattering, will be uncorrelated to the total jet momentum created from the hard scattering, and at mid rapidity most high p_T-jets come from FSR. On average the ISR contribution will be constant, meaning that the ratio would decrease for higher jet-p_T. It is also seen that ISR contribution is increased for higher rapidities, for both pp and PbPb collisions. This is because the ISR radiation will tend to be collinear with the beam axis since it is emitted before the hard-scattering. This means that it will be concentrated at forward rapidities.

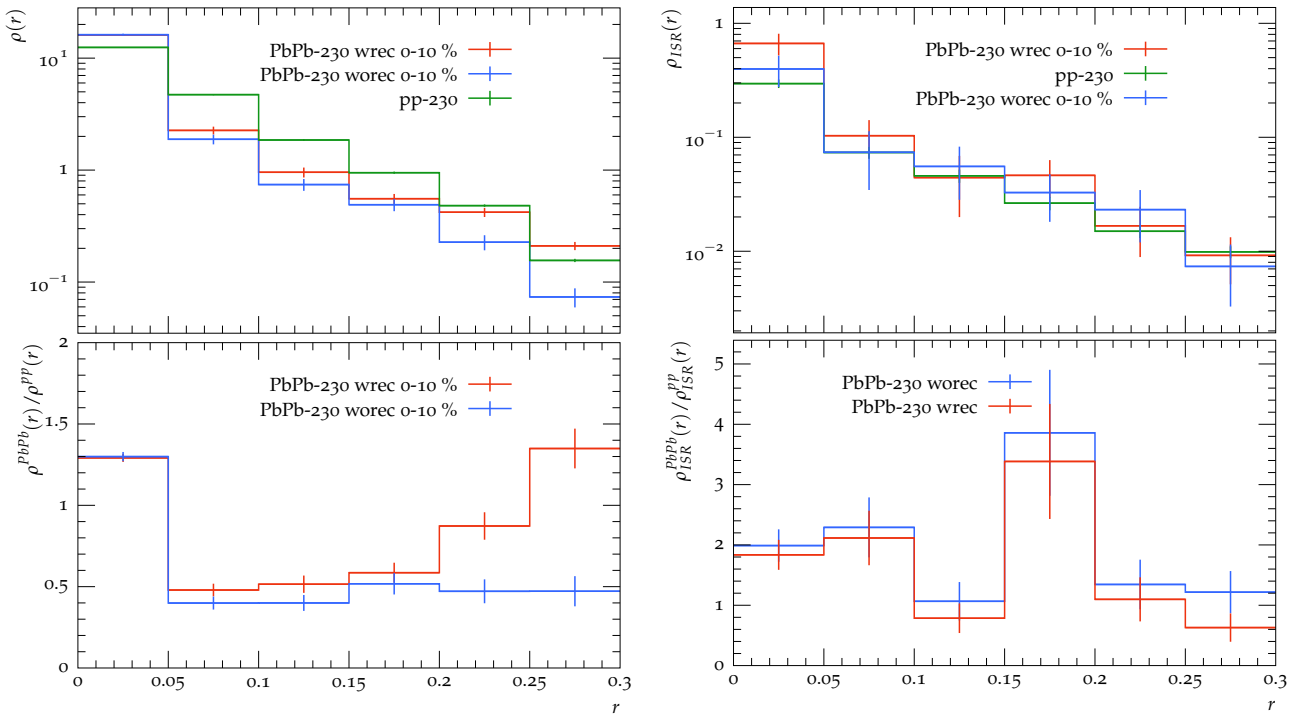

Figure 8: The jet-shape (left) and ISR jet-shape (right) are plotted in top figures, and nuclear modification factors are plotted in the bottom figures for different distances r from the jet axis.

In figure 8, it is seen that the inclusive (i.e. total) jet shape is decreasing exponentially for all collisions. This is expected in a jet since the majority of the energy and momentum will be concentrated at smaller distances r. The ISR jet-shape looks very similar to the regular jet shape in this plot which is rather surprising. If the ISR contribution is assumed to be constant, then the ISR jet-shape should not fall exponentially in this manner. One reason as to why the ISR jet-shape is so similar to the inclusive jet-shape could be due to there being a lot of jets having high p_T contributions (more than half of the p_T comes from ISR). But as is seen by comparing the nuclear modification factor for the ISR jet-shape and the inclusive jet-shape, the ratios are not the same. It is expected that the nuclear modification factor should increase for larger distances r, which is due to the fact that the contributions from the medium response have a much broader distribution than the jet. This is because the contributions from medium response are relatively soft in transverse momentum but at large angles from the beam axis.

4.1.2 Results with $\sqrt{s_{NN}} = 2.76$ TeV & JEWEL-240

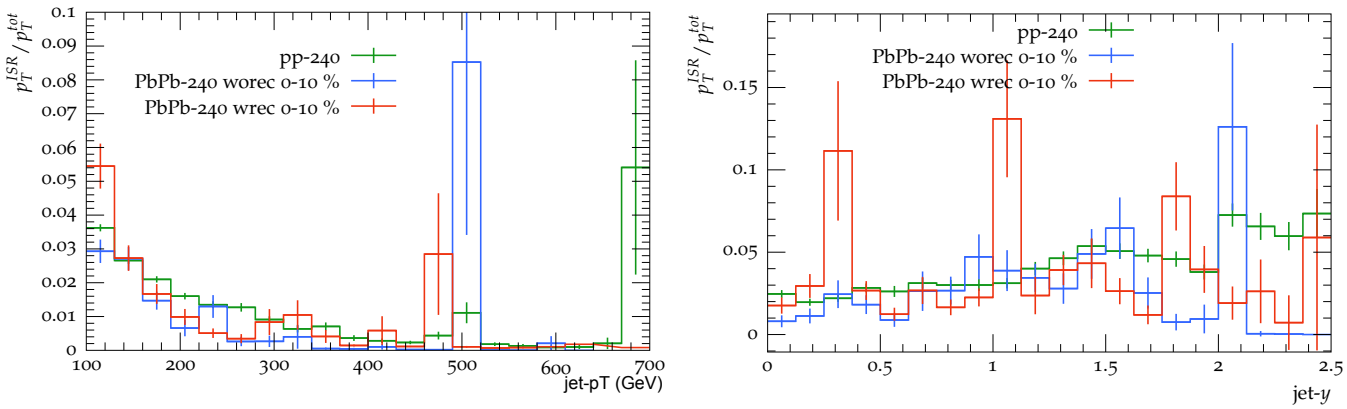

Figure 9: The ISR jet-p_T fraction is plotted for different jet-p_T and jet-y in pp-collisions (green lines) and in $PbPb$-collisions with JEWEL-240. HIC with medium response correspond to red lines, and without medium response correspond to blue lines.$\sqrt{s_{NN}} = 2.76$ TeV

The p_T contribution in figure 9 looks quite similar to the one in JEWEL-230. One big difference however is that the PbPb collisions that are created without medium response, is significantly smaller than with JEWEL-230. This is because with JEWEL-240, the ISR can also be "quenched", resulting in a noticeable p_T loss. This results into the ISR-p_T contribution being less than pp collisions. Possibly indicating that the ISR particles interact more with the medium than the FSR ones. There is also a large sudden increase in p_T at around 500 GeV. This kind of fluctuation happens once more in figure 17 at roughly the same p_T, but there is no clear indication as to why that would happen. Due to the high error-bars, this is likely just a random fluctuation.

Figure 9 also shows an increase in ISR-p_T contribution for higher rapidities. However, in PbPb collisions with medium response, the contribution fluctuates quite considerably and it is hard to see if it actually increases for higher rapidities. This could be due to the constituent subtraction that is performed when keeping the thermal particles, i.e. medium response. While this wouldn't change the rapidity of the particles, it would change p_T and m_T, meaning that the ISR yields different contributions at different rapidities, as compared to when medium response is not included.

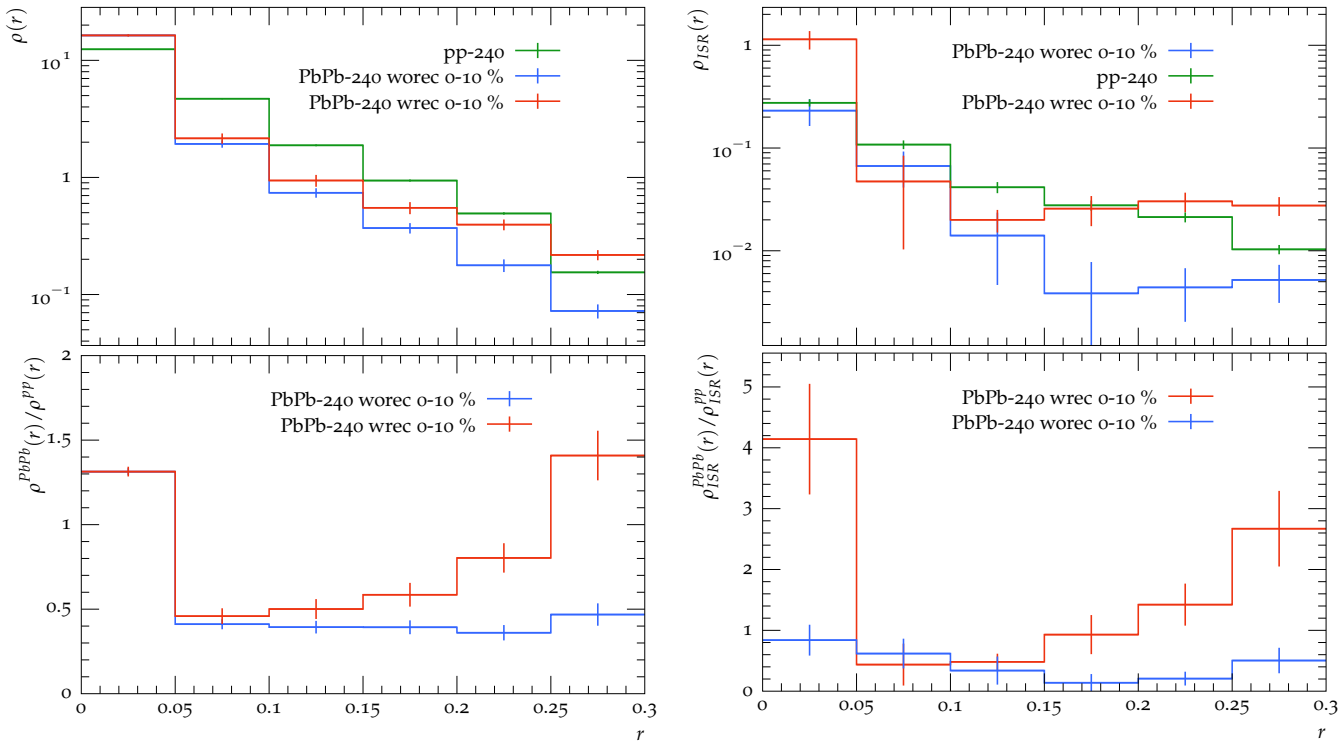

Figure 10: The inclusive jet-shape and ISR jet-shape are plotted in top figures, and the jet shape nuclear modification factors is shown in the bottom for different distances r from the jet axis.

In figure 10, the ISR jet-shape does not fall off in the same way as for JEWEL-230. As is seen, for larger distances r, the graph becomes pretty flat, which as discussed earlier could be because there are not very many initial state jets. This can probably be explained by the fact that the ISR particles now interact with the thermal particles. An interesting observation is in the ISR nuclear modification factor, where it is seen that the ratio for events without medium response is below 1 for all r, but not so for events with medium response. The PbPb-240 wrec, increases with higher r, which essentially means that ISR located far outside the jet-axis is less quenched. The reason why it is higher for small r is because the ISR interactions are hard or semi-hard close to the jet axis.

4.1.3 Results with $\sqrt{s_{NN}} = 5.02$ TeV & JEWEL-230

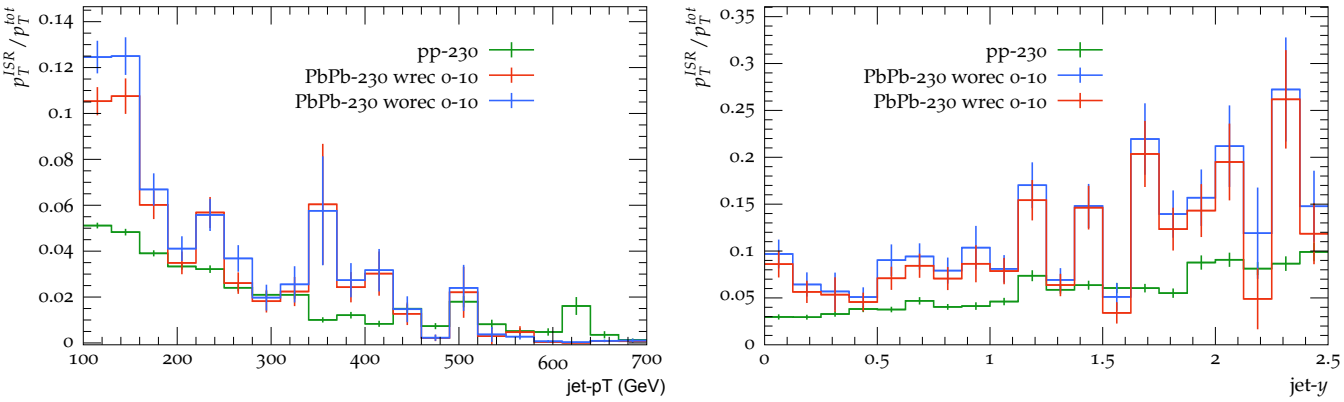

Figure 11: The ISR jet-p_T fraction is plotted for different jet-p_T and jet-y in pp-collisions (green lines) and in $PbPb$-collisions with JEWEL-230. HIC with medium response correspond to red lines, whereas without medium response correspond to blue lines. $\sqrt{s_{NN}} = 5.02$ TeV

The most apparent difference between the p_T graph in figure 11 and figure 7, is that the ISR-p_T contribution doesn't fall off as fast for higher p_T in figure 11. This is because of the increase

in beam energy, which also affects the energy the ISR can have. The ISR-p_T is also higher for the PbPb collisions, especially events without medium response. This seems to indicate that the FSR interacts more strongly with the medium for higher beam-energies since the energy reduction is greater. This is because higher beam-energy means that the medium is denser and exists for a longer duration. Higher contributions for larger p_T also imply that the jets are more suppressed for higher p_T, as is apparent by the comparison. The surprising remark is that this is also true in pp collisions. This means that the increase in energy affects the ISR more than the FSR.

In figure 11, as opposed to the other y graphs, a very clear increase can be seen for all the collisions for increasing rapidities. And at mid-range rapidities the ISR-p_T contribution becomes quite sizeable.

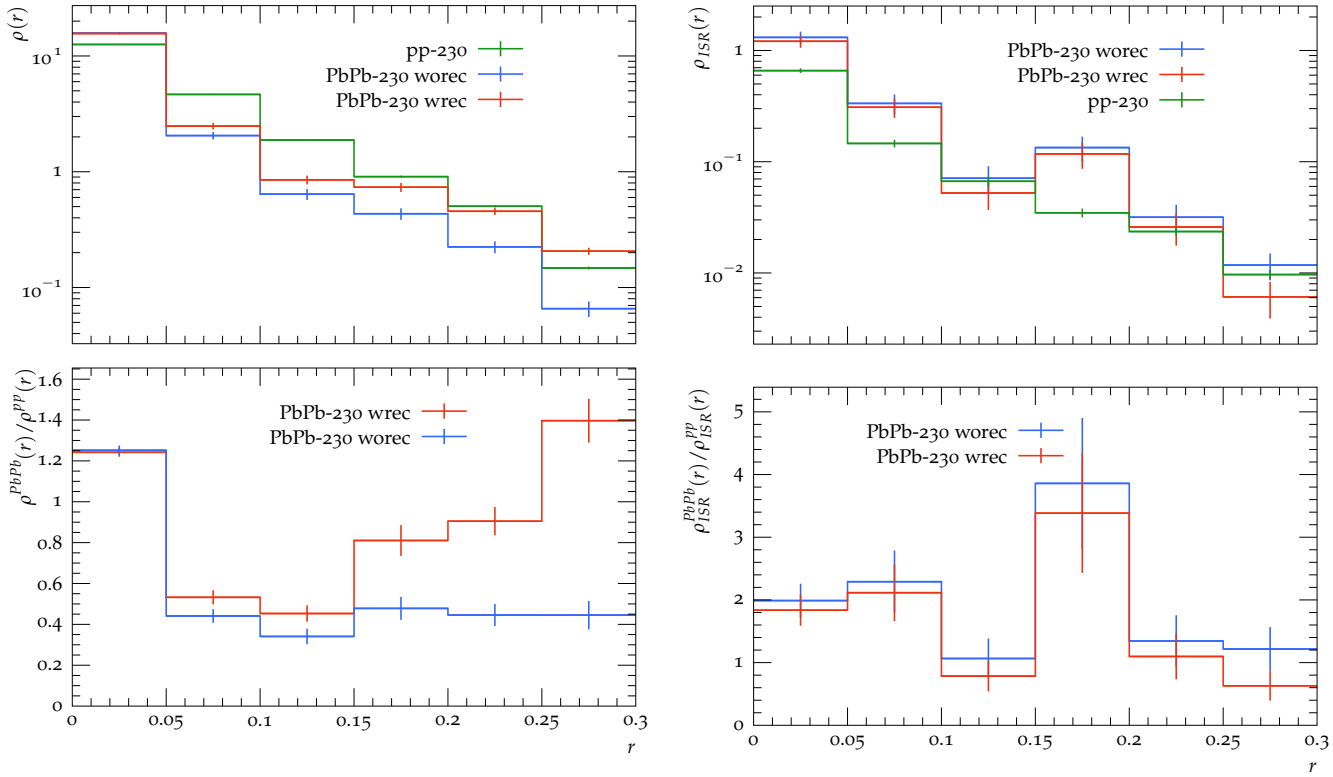

Figure 12: The jet-shape and ISR jet-shape are plotted in top figures, whereas the jet shape nuclear modification factors are plotted in the bottom figures for different distances r from the jet axis.

In figure 12, the inclusive jet-shape looks almost identical to the one in figure 8 in both shape and values. The ISR jet-shape looks fairly similar between the two set of events, but there are a few differences. One major difference is that there is a large noticeable bump between $0.15 < r < 0.2$, which is there for both PbPb collisions with and without medium response. This bump, although smaller, can be seen in figure 8 aswell for PbPb collisions with medium response, but not for PbPb without recoiling particles. It's unclear why this happens, but it is likely due to statistical errors.

Another key difference is that for the ISR jet shape, the values are quite a bit higher compared to those in figure 8. This could be due to either the jet quenching having a larger effect on the jet at this energy or due to the ISR-p_T contribution increasing for higher energies.

4.1.4 Results with $\sqrt{s_{NN}} = 5.02$ TeV & JEWEL-240

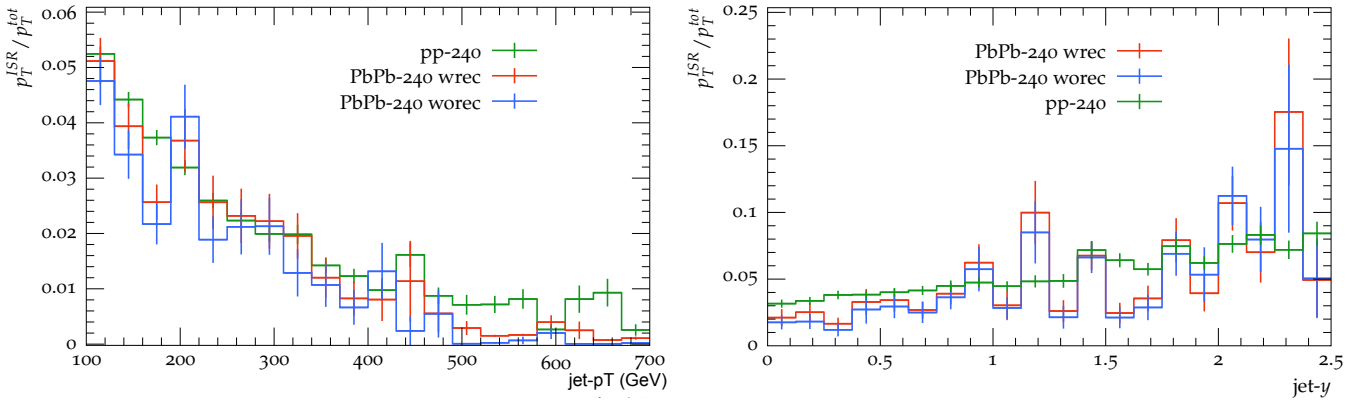

Figure 13: The ISR jet-p_T fraction is plotted for different jet-p_T and jet-y in pp-collisions (green) and in $PbPb$-collisions with JEWEL-240. HIC with medium response correspond to red lines, whereas without medium response correspond to blue lines. $\sqrt{s_{NN}} = 5.02$ TeV

In figure 13, the ISR-p_T contribution is once again heavily reduced due to the ISR being able to interact with the thermal particles. What's interesting for this figure however is that in both of the PbPb collisions, the average ISR-p_T contribution is lower compared to the pp-collisions. This is true for all p_T but is most noticeable at 500 - 700 GeV. This is different from figure 9, where the PbPb with recoiling particles has the largest contribution. This is in contradiction with the previous point made for the $\sqrt{s_{NN}} = 5.02$ TeV & JEWEL-230 events, where it was suggested that the FSR interact more with the medium.

Another observation to be made is that the ISR contribution increases quite steadily with increasing rapidity. The contribution is also higher on average for $\sqrt{s_{NN}} = 5.02$ TeV as compared to $\sqrt{s_{NN}} = 2.76$ TeV.

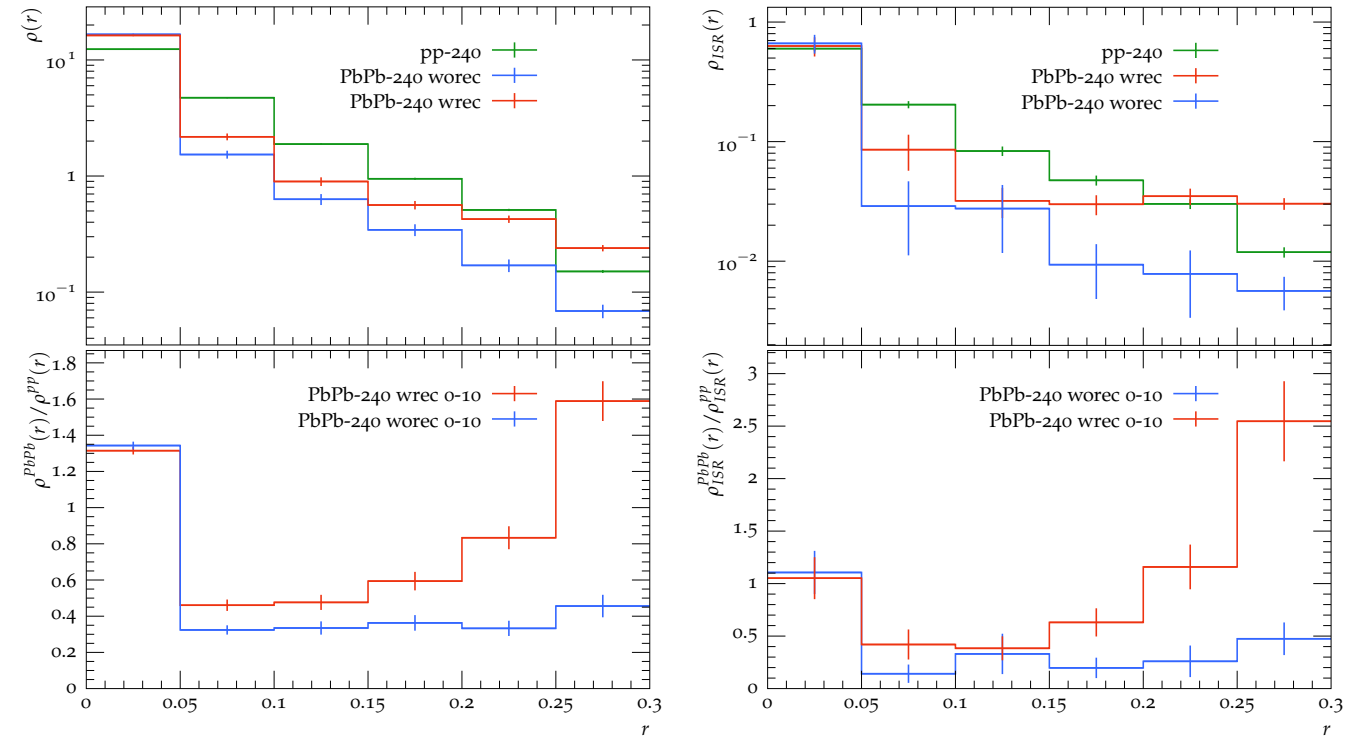

Figure 14: The jet-shape and ISR jet-shape are plotted in top figures and the jet shape nuclear modification factors are plotted in the bottom figures for different distances r from the jet axis.

Once again, there is not too much difference in the inclusive jet shape and the inclusive nuclear modification between $\sqrt{s_{NN}} = 5.02$ TeV and $\sqrt{s_{NN}} = 2.76$ TeV. The ISR jet shape in figure 14 looks slightly different from figure 10. In both cases, there is a non-exponential decay for the PbPb interactions, but the nuclear modification factor is larger in average for the $\sqrt{s_{NN}} = 2.76$ TeV events.

4.2 Results for large jets (R = 1.0)

4.2.1 Results with $\sqrt{s_{NN}} = 2.76$ TeV & JEWEL-230

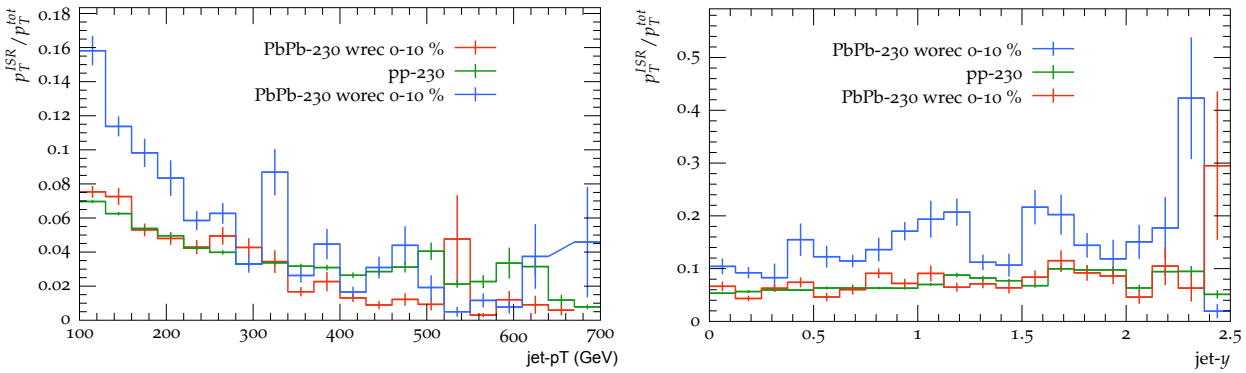

Figure 15: The ISR jet-p_T fraction is plotted for different jet-p_T and jet-y in pp-collisions and $PbPb$-collisions. JEWEL-230, $\sqrt{s_{NN}} = 2.76$ TeV

It is clear in figure 15, that with higher jet radius, more particles will be picked up by the jets and since the ISR are not quenched, there will be an increase in the ISR-p_T contribution as compared to figure 7. This is especially true when there is no medium response. One difference between the two graphs is however that the PbPb with medium response, has almost the same ISR-p_T contribution as in the pp collisions. This is because the thermal particles are spread out consistently over the QGP area, meaning that an increased jet radius will also pick up more thermal particles. This then lowers the ISR contribution since the thermal contribution to the jet-p_T increases. The rapidity graph looks fairly similar except that, the contribution from the PbPb wrec is reduced when $R = 1.0$.

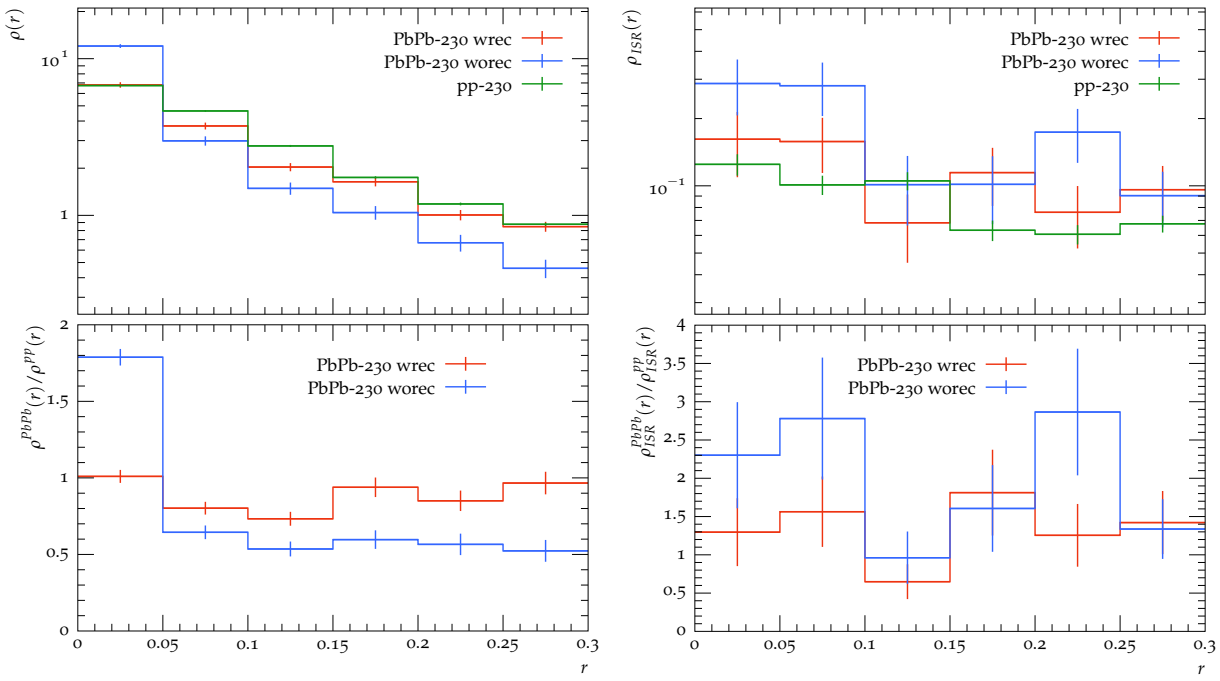

Figure 16: The jet-shape and ISR jet-shape are plotted for different distances r from the jet axis.

Figure 16 shows that both the inclusive- and the ISR jet-shape is different from that in figure 8. In PbPb collisions with recoil, the jet shape is noticeably reduced with $R = 1.0$. The nuclear modification factor is approximately 1 for all r. This is actually something that is observed in all the $R = 1.0$ plots, with slight variations. This is because the average p_T is increased for large distance from all the thermal particles and since the jet shape is an average, it means that it will go down for smaller distances. The ISR jet shape differs quite drastically compared to that in figure 8. With $R = 0.3$, the ISR jet-shape matched the inclusive jet-shape fairly well and decreased exponentially for larger r. With $R = 1.0$, the jet shape is relatively flat for larger r and does not decrease significantly and it does have some enhancement close to the jet axis. The enhancement is as said previously due to the ISR from interactions that are semi-hard/hard, giving it a more typical jet shape.

4.2.2 Results with $\sqrt{s_{NN}} = 2.76$ TeV & JEWEL-240

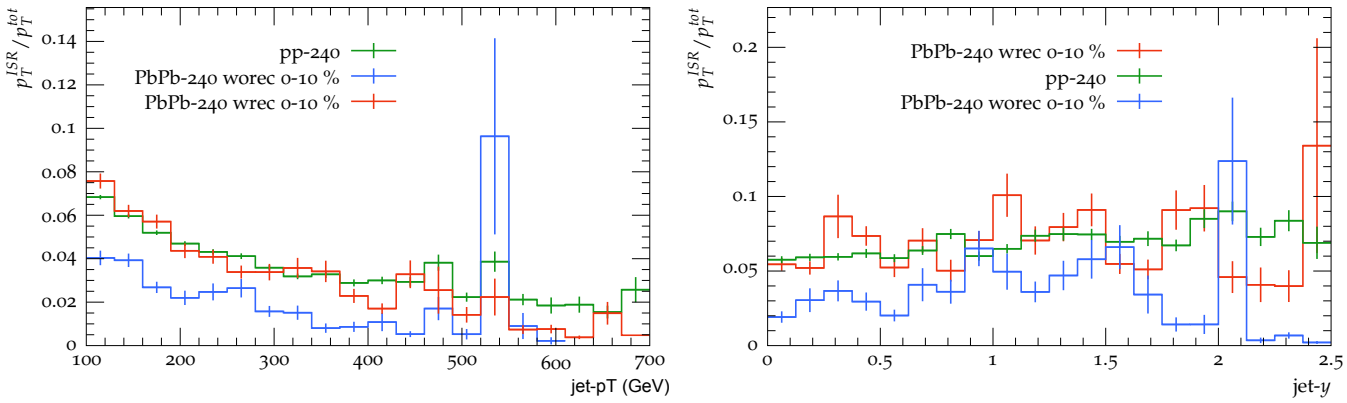

Figure 17: The ISR jet-p_T fraction is plotted for different jet-p_T and jet-y in pp-collisions (green) and in $PbPb$-collisions with JEWEL-240. HIC with medium response correspond to red lines, whereas without medium response correspond to blue lines. $\sqrt{s_{NN}} = 2.76$ TeV

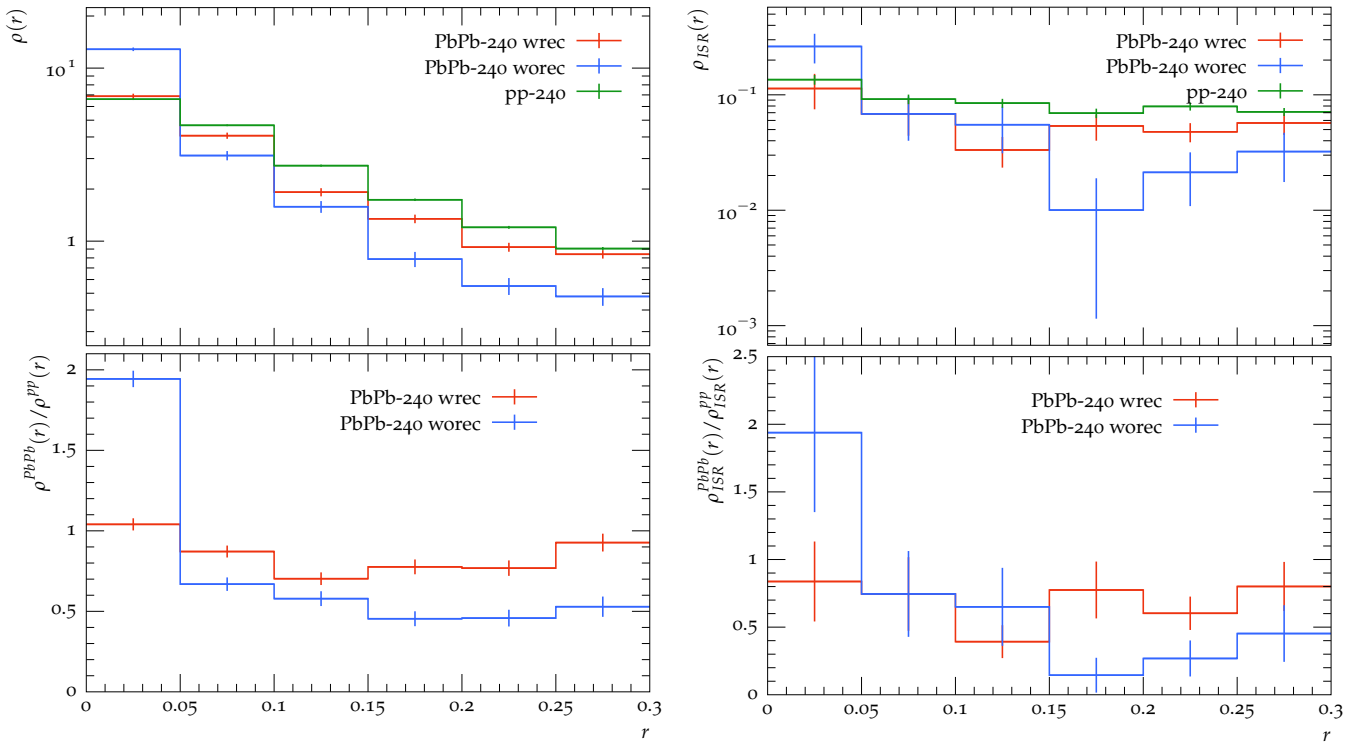

Figure 18: The jet-shape and ISR jet-shape are plotted in top figures, and the jet shape nuclear modification factors are plotted in the bottom figures for different distances r from the jet axis.

When the ISR can interact with the medium, the largest difference is that the ISR-p_T contribution actually increases slightly, and does not fall off as fast for higher p_T's. This is observed by comparing figure 17 with 9. It is seen that in figure 17, PbPb collisions without thermal particles included, have a far smaller ISR-p_T contribution. This is because the ISR are concentrated around the beam axis, meaning that the FSR will interact more with the medium and thus lose more energy. This same reason causes the increase in the ISR contribution for increasing rapidity as well. The inclusive jet-shapes and the ISR jet-shapes actually differ very little as seen when comparing figure 18 and figure 10. In $R = 1.0$, the nuclear modification factors are reduced for PbPb collisions with medium response in both the inclusive jet-shape and the ISR jet-shape. At the same time the PbPb collisions without medium responce is enhanced for the different r with $R = 1.0$.

4.2.3 Results with $\sqrt{s_{NN}} = 5.02$ TeV & JEWEL-230

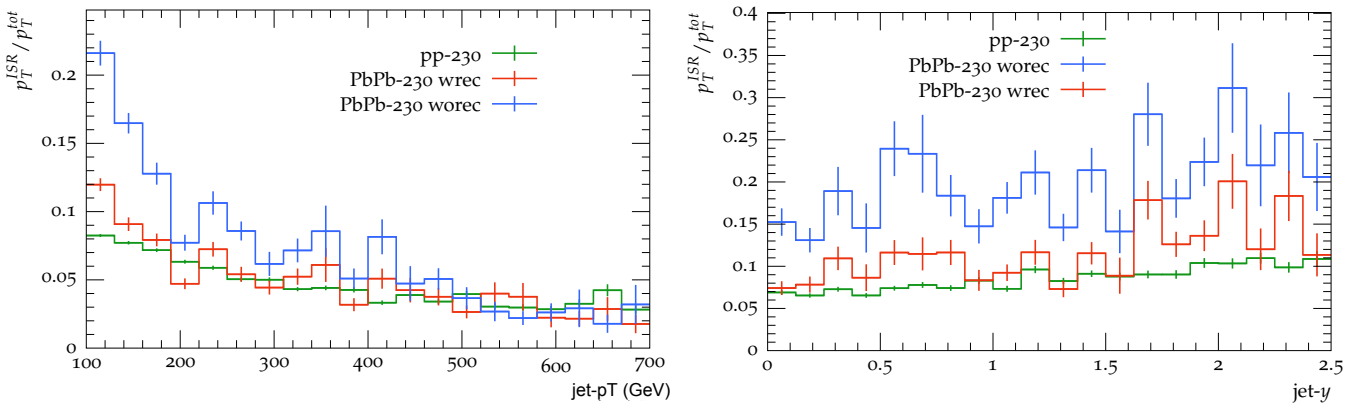

Figure 19: The ISR jet-p_T fraction is plotted for different jet-p_T and jet-y in pp-collisions (green) and in $PbPb$-collisions with JEWEL-230. HIC with medium response correspond to red lines, whereas without medium response correspond to blue lines. $\sqrt{s_{NN}} = 5.02$ TeV

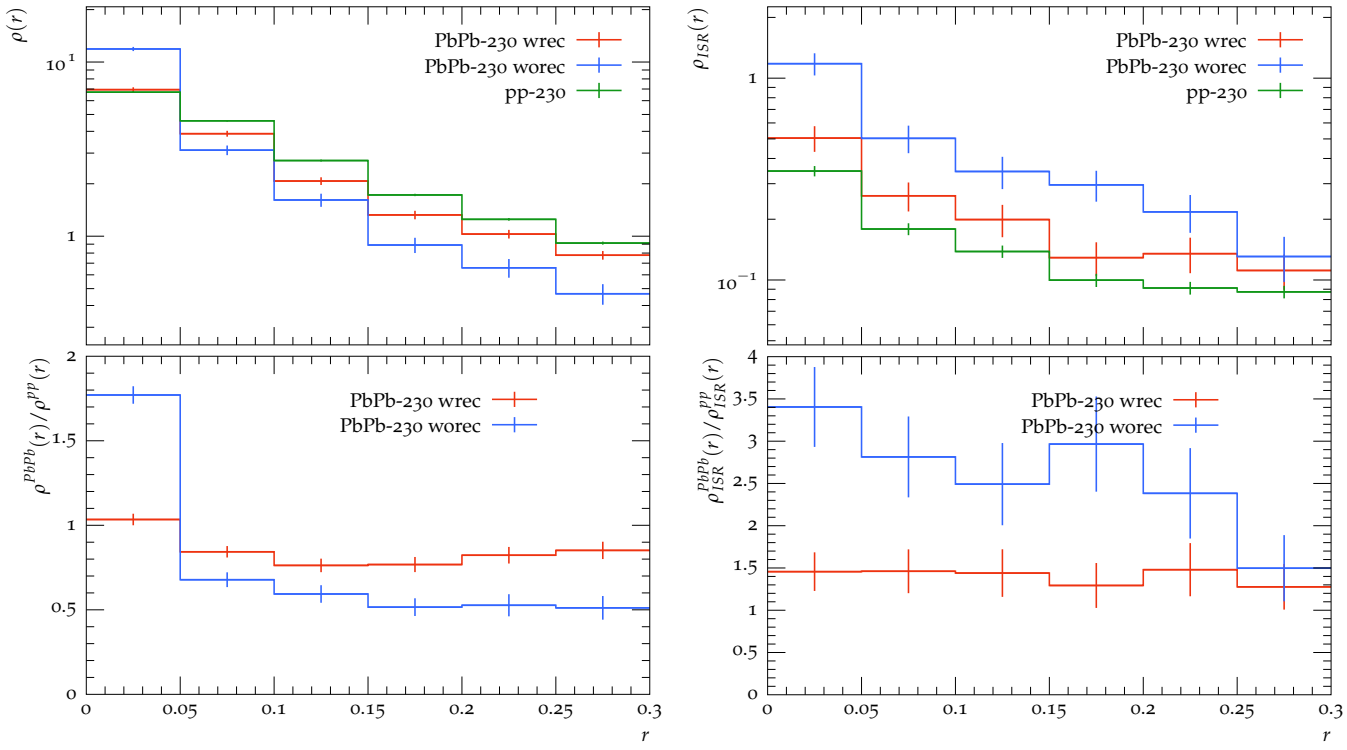

Figure 20: The jet-shape and ISR jet-shape are plotted in the top figures and the jet shape nuclear modification factors are plotted in the bottom figures for different distances r from the jet axis.

Comparing the ISR-p_T contribution for the same beam-energy and JEWEL version it can be seen that figure 19 differs from figure 11 in the same points as covered before. Since ISR can not interact with the medium, and thus not be quenched, a larger ISR-p_T contribution is expected. Because of the increasing jet radius, the FSR particles will interact with more thermal particles, and if these are not then included, then obviously the ISR-p_T contribution will increase for higher R. For the same reason there will also be an increase for higher rapidities which is also observed. The inclusive jet shape and the ISR jet shape also looks pretty much like it is expected in figure 20. The contributions in PbPb wrec are heavily reduced due the massive increase of thermal particles, whereas without thermal particles, the contributions will increase since the total jet-p_T will decrease, but the ISR-p_T will remain unchanged. It is observed that for higher jet radius, the ISR jet-shape also starts to look less jet-like.

4.2.4 Results with $\sqrt{s_{NN}} = 5.02$ TeV & JEWEL-240

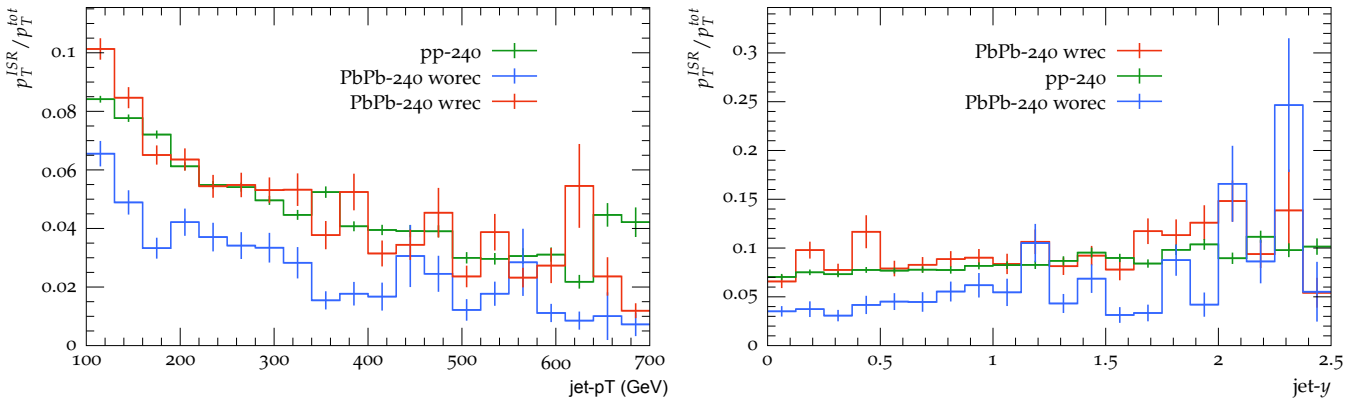

Figure 21: The ISR jet-p_T fraction is plotted for different jet-p_T and jet-y in pp-collisions (green) and in $PbPb$-collisions with JEWEL-240. HIC with medium response correspond to red lines, whereas without medium response correspond to blue lines. $\sqrt{s_{NN}} = 5.02$ TeV

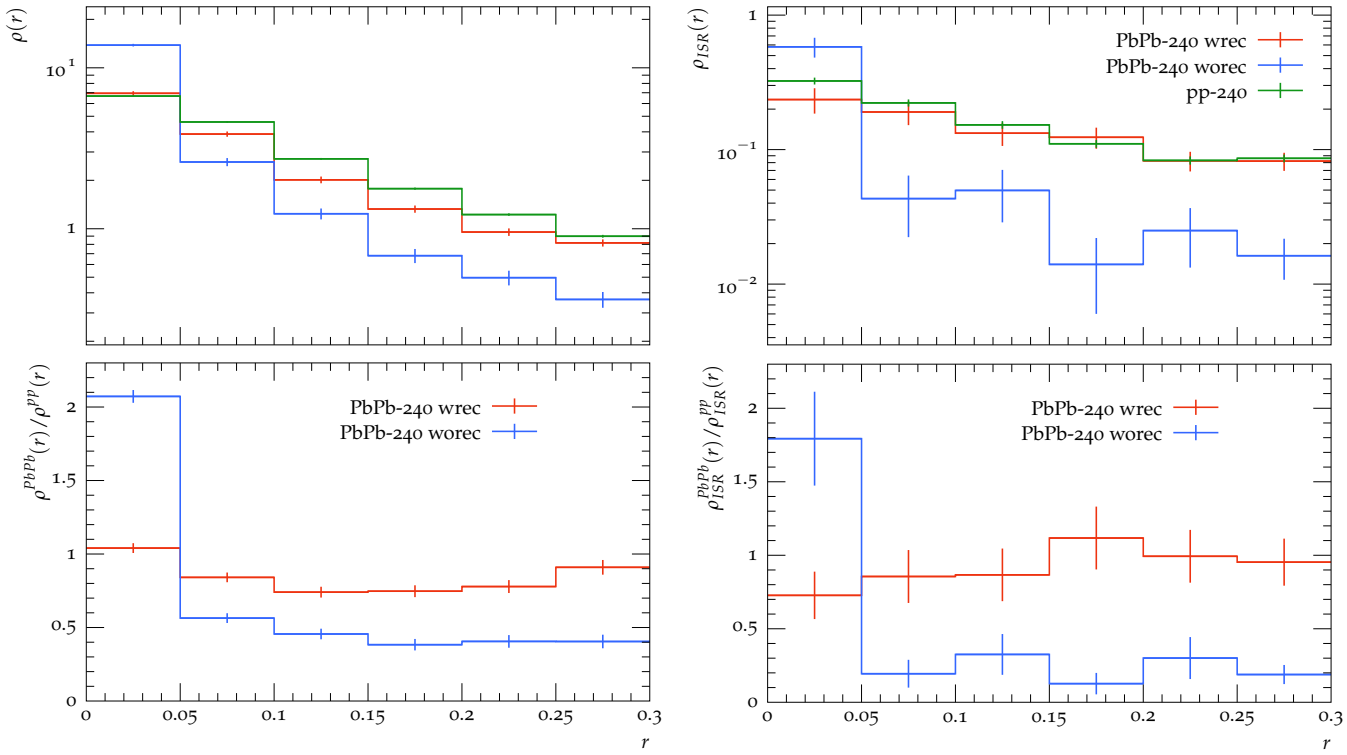

Figure 22: The jet-shape and ISR jet-shape are plotted in top figures and the jet shape nuclear modification factors are plotted in the bottom figures for different distances r from the jet axis.

Comparing figure 21 with figure 13, it is seen that the ISR-p_T contributions are higher for $R = 1.0$. This is because the ISR will tend to be close to the jet axis, meaning that it is mostly the FSR that interact with the thermal particles. FSR particles will thus lose more of their momentum in large jets which means that the ISR contribution increases. The same can be said about the ISR contribution for different rapidities. Looking at figure 22 and figure 14, it can be seen that the ISR jet shape looks less "jet-like" for $R = 1.0$. Further, just as in the previous case, the nuclear modification factor will be reduced for PbPb collisions with medium response and increase for collisions without medium response. This is due to the same reasons as mentioned in section 4.2.3.

Different centralities were also examined for events where $\sqrt{s_{NN}} = 2.76$ TeV and $R = 0.3$, but no strong correlation on how the ISR-p_T contribution was changed could be made. Therefore these are not included in the main body but instead can be found in the appendix. As is seen from e.g. comparing figure 9 and figure 25, the contributions seem almost identical.

5 Conclusion

The main take-away from analysing all of these graphs is that the initial state radiation does not affect the jet-p_T significantly. The contributions from the initial state radiation are in the order of a few percent, and will not affect the jets in a global scale. The initial state contributions are largest for small p_T-jets (i.e. 100 - 300 GeV) and decreases pretty fast for increasing p_T. This is because the ISR contribution is assumed to be constant on average, meaning that increasing jet-p_T, decreases the contribution. It was also shown that the ISR contribution was largest for high er rapidities. For some of the plots, e.g. 17, the ISR contribution reached 15-25 % for rapidities between $2 < y < 2.5$. This could be explained by the fact that most of the FSR is concentrated at low/mid range rapidities, whereas the ISR is concentrated at forward rapidities.

It was observed that increasing the jet radius yields a larger contribution from the initial state radiation to the jet's p_T. Increasing the beam energy also increased the initial state contribution to the jet-p_T, but by a far smaller factor. For instance, when comparing events with two different jet radius but with the same energy, e.g. figure 21 and figure 13, it can be seen that the initial state contribution is almost doubled. Whereas, comparing events where the jet radius is the same but the energy is different, e.g. figure 17 and 21, an increase in the ISR contribution could be seen for the higher-energy events, but it is only by 10-20 %. This increase in initial state contribution to the jet-p_T is both recorded for different values for the jet-p_T and for different rapidities. The centralities of the collisions did not seem to affect the results. This however, was not adequately tested for $R = 1.0$.

It was also observed that in events where the initial state radiation could interact with the thermal particles in the medium, the nuclear modification factors for the ISR jet-shape varied quite dramatically, depending on if medium response was included or not. The exact effect from the medium response depends mostly on the jet radius, but an example would be figure 10, where it can be seen that the medium response increases the ratio $\rho_{ISR}^{PbPb}(r)/\rho_{ISR}^{pp}(r)$ for increasing r. This is because the ISR is concentrated around the jet axis, meaning that the ISR will not interact with the QGP state as much as the FSR. On the other hand for a large jet radius, e.g. $R = 1.0$, the effects from the medium response does not seem to affect the contribution of the ISR to the jet-p_T.

It is clear that large jet radii are needed with high energies to be able to study the contri-

bution from the initial state radiation to the jet structure as effectively as possible. Many experiments today are pushing very hard to reconstruct large radius jets in PbPb collisions. This allows for a more detailed investigation of primarily the medium response- but also the initial state -contribution to the jet structure. These come hand-in-hand since they are both broadly distributed, with a weak correlation to the jet. This means that in real experiments, a sense of caution has to be employed when interpreting results for high jet radii, since it is not very clear what contributions come from the medium response and what comes from initial state radiation.

There are quite a few improvements and some interesting investigations that could be made in the future (however, because of limits in the size of the thesis, many had to be omitted in this thesis). A major improvement is to increase the number of events produced for mainly the PbPb events. While 100000 events are adequate for some measurements, it is clear that there are quite a bit of fluctuations for other measurements. An adequate number would be a e.g. a million events or more instead.

Because of the limitations of technology, data sets do not exist for beams with higher energies, but it would be interesting to see how much the initial state contribution would be affected if analyses could be done for even higher energies than 5.02 TeV. Having larger jet radii is a bit unrealistic, but instead differet jet substructure observables could have been studied for the jet radius $R = 1.0$.

Acknowledgements

First and foremost, I want to thank my supervisor Korinna Zapp for her constant support and feedback in this thesis and for introducing me to heavy ion physics. I also want to thank my family and friends who have supported me. Lastly, I want to thank everyone at the Lund Theoretical Physics division.

Appendix

A 30 - 50 % centrality (R = 0.3)

A.1 $\sqrt{s_{NN}} = 2.76$ TeV & JEWEL-230

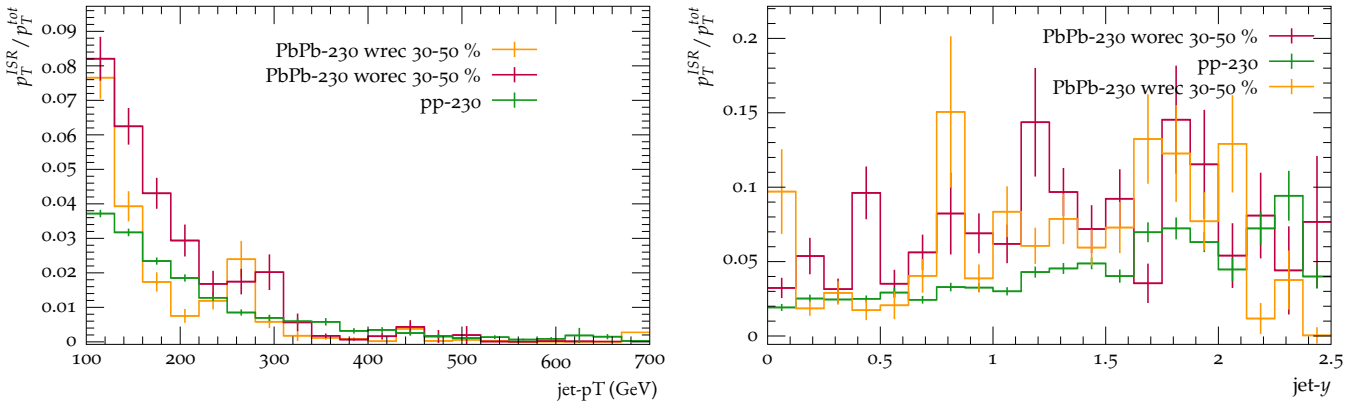

Figure 23: The ISR jet-p_T fraction is plotted for different jet-p_T and jet-y in pp-collisions (green) and in $PbPb$-collisionswith JEWEL-230. HIC with medium response correspond to orange lines, whereas without medium response correspond to purple lines. $\sqrt{s_{NN}} = 2.76$ TeV

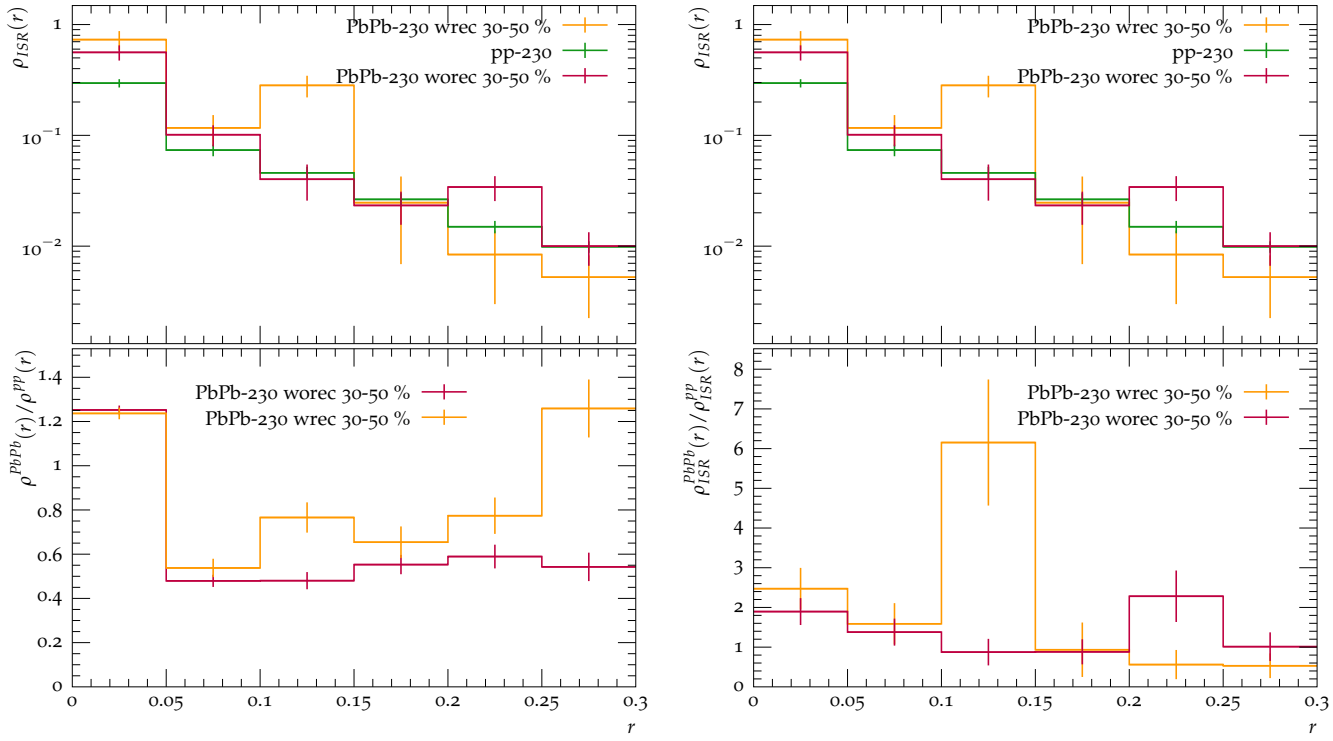

Figure 24: The jet-shape and ISR jet-shape are plotted in top figures, whereas the jet shape nuclear modification factors are plotted in the bottom figures for different distances r from the jet axis.

A.2 $\sqrt{s_{NN}} = 2.76$ TeV & JEWEL-240

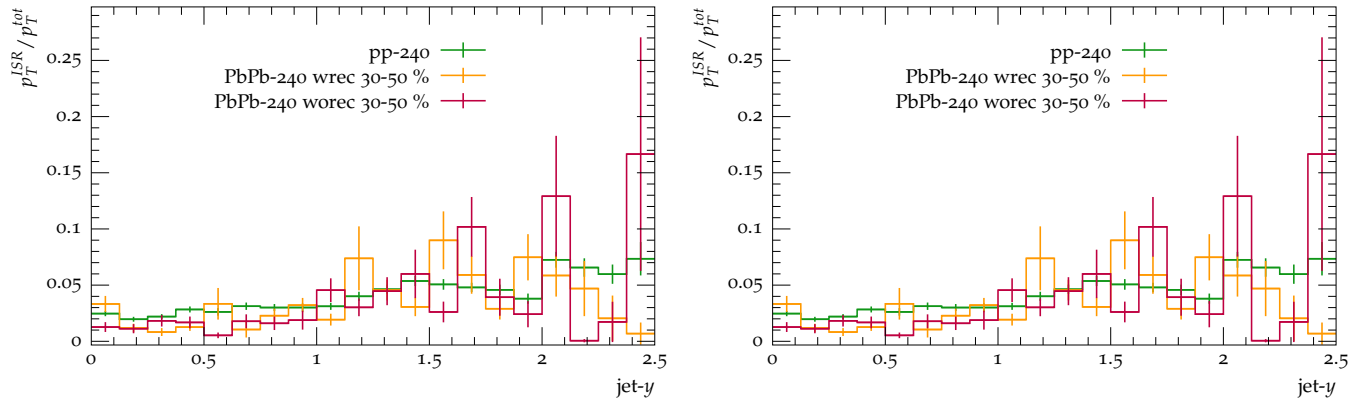

Figure 25: The ISR jet-p_T fraction is plotted for different jet-p_T and jet-y in pp-collisions (green) and in $PbPb$-collisions with JEWEL-240. HIC with medium response correspond to orange lines, whereas without medium response correspond to purple lines. $\sqrt{s_{NN}} = 2.76$ TeV

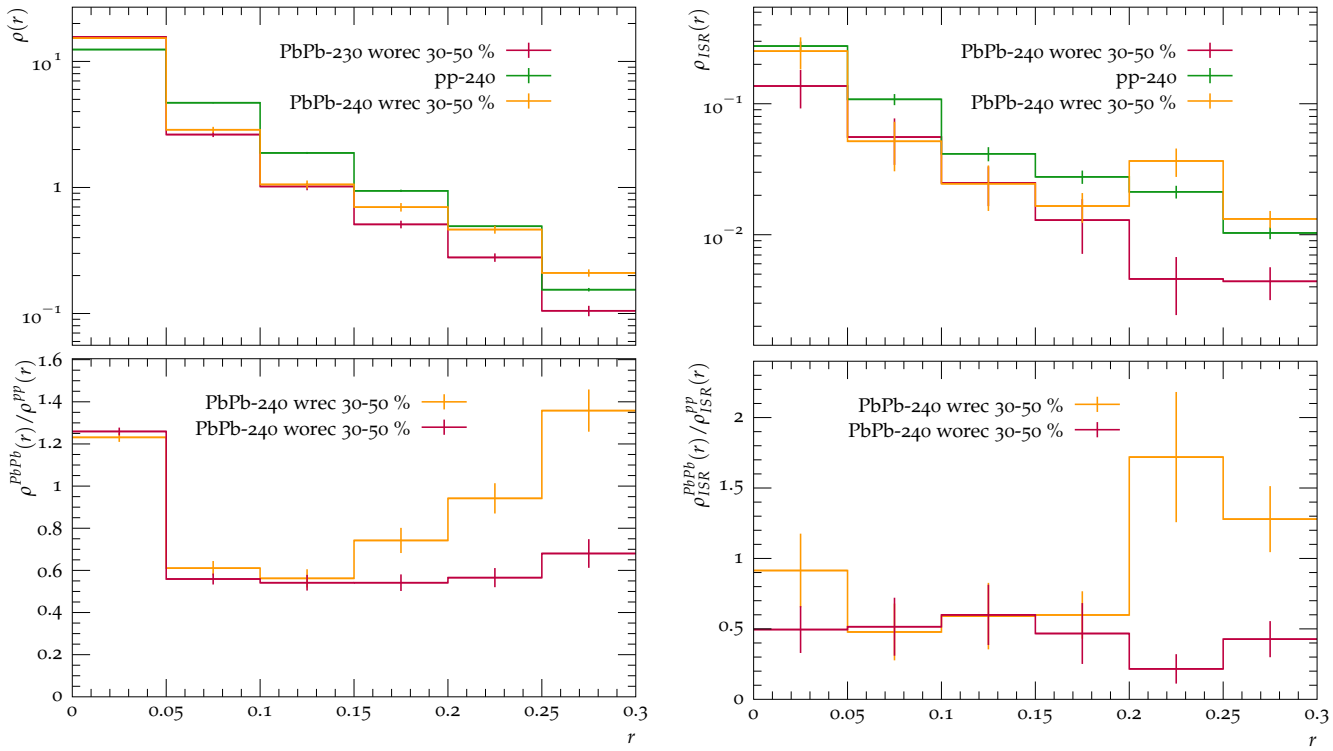

Figure 26: The jet-shape and ISR jet-shape are plotted in top figures, whereas the jet shape nuclear modification factors are plotted in the bottom figures for different distances r from the jet axis.

B 70 - 100 % centrality (R = 0.3)

B.1 $\sqrt{s_{NN}} = 2.76$ TeV & JEWEL-230

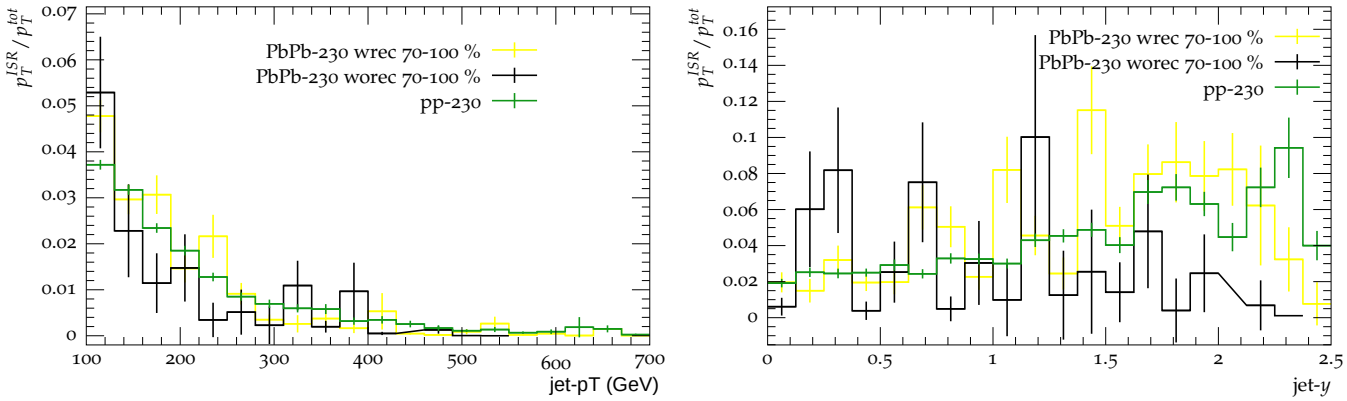

Figure 27: The ISR jet-p_T fraction is plotted for different jet-p_T and jet-y in pp-collisions (green) and in $PbPb$-collisions with JEWEL-230. HIC with medium response correspond to black lines, whereas without medium response correspond to yellow lines. $\sqrt{s_{NN}} = 2.76$ TeV

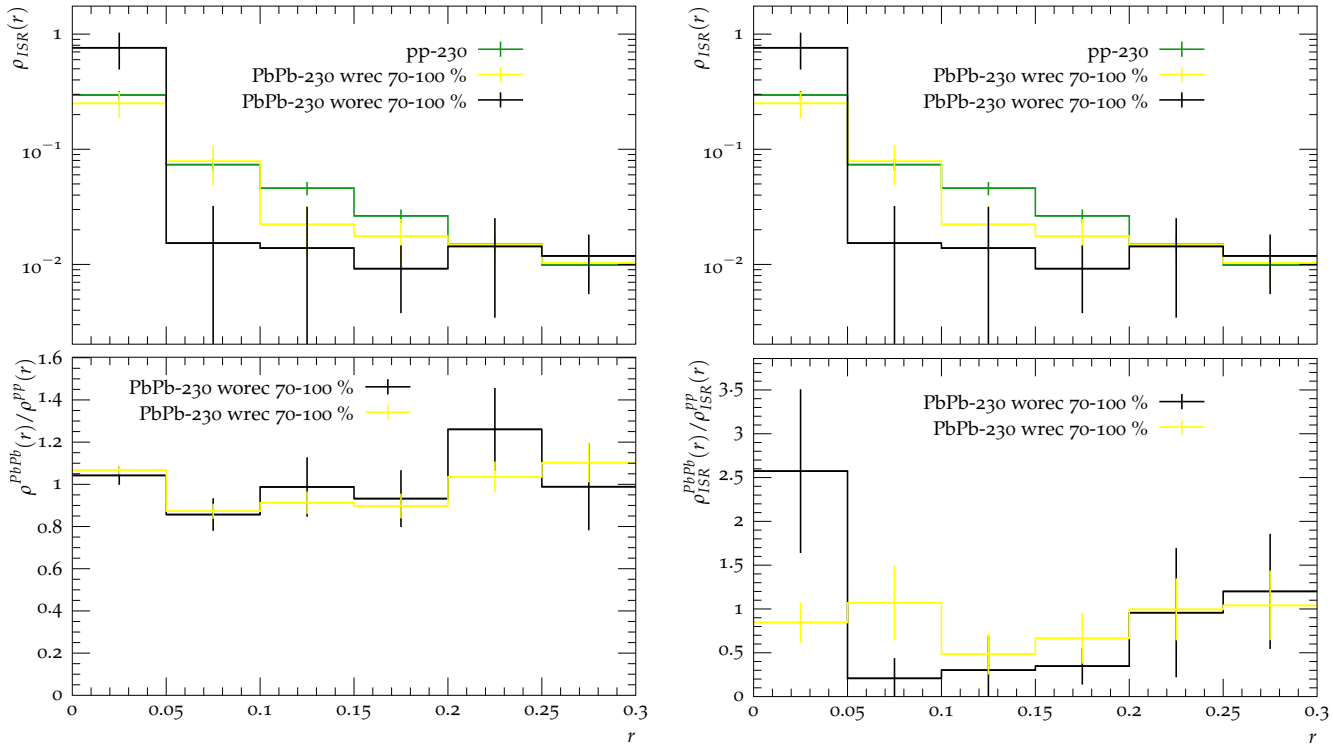

Figure 28: The jet-shape and ISR jet-shape are plotted in top figures, whereas the jet shape nuclear modification factors are plotted in the bottom figures for different distances r from the jet axis.

B.2 $\sqrt{s_{NN}} = 2.76$ TeV & JEWEL-240

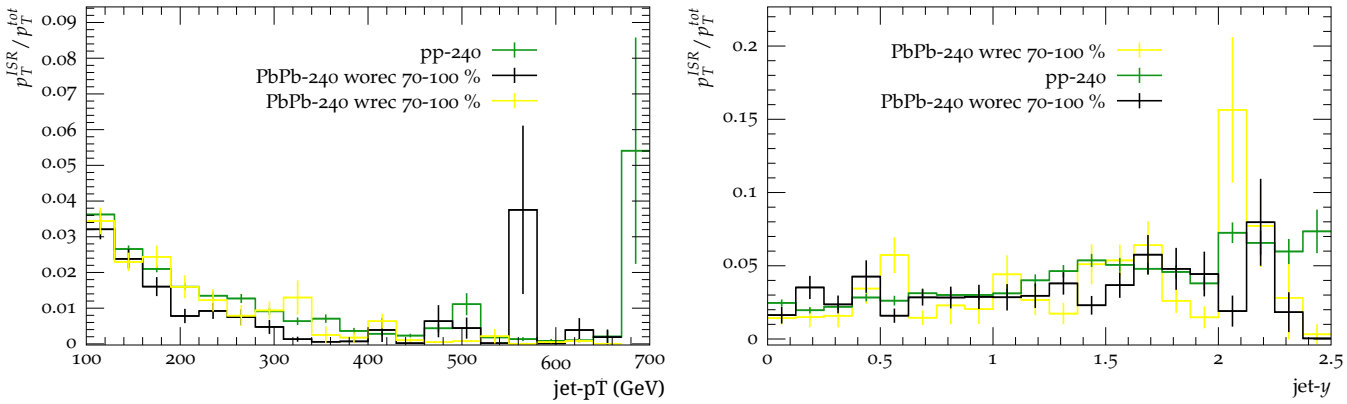

Figure 29: The ISR jet-p_T fraction is plotted for different jet-p_T and jet-y in pp-collisions (green) and in $PbPb$-collisions with JEWEL-240. HIC with medium response correspond to black lines, whereas without medium response correspond to yellow lines. $\sqrt{s_{NN}} = 2.76$ TeV

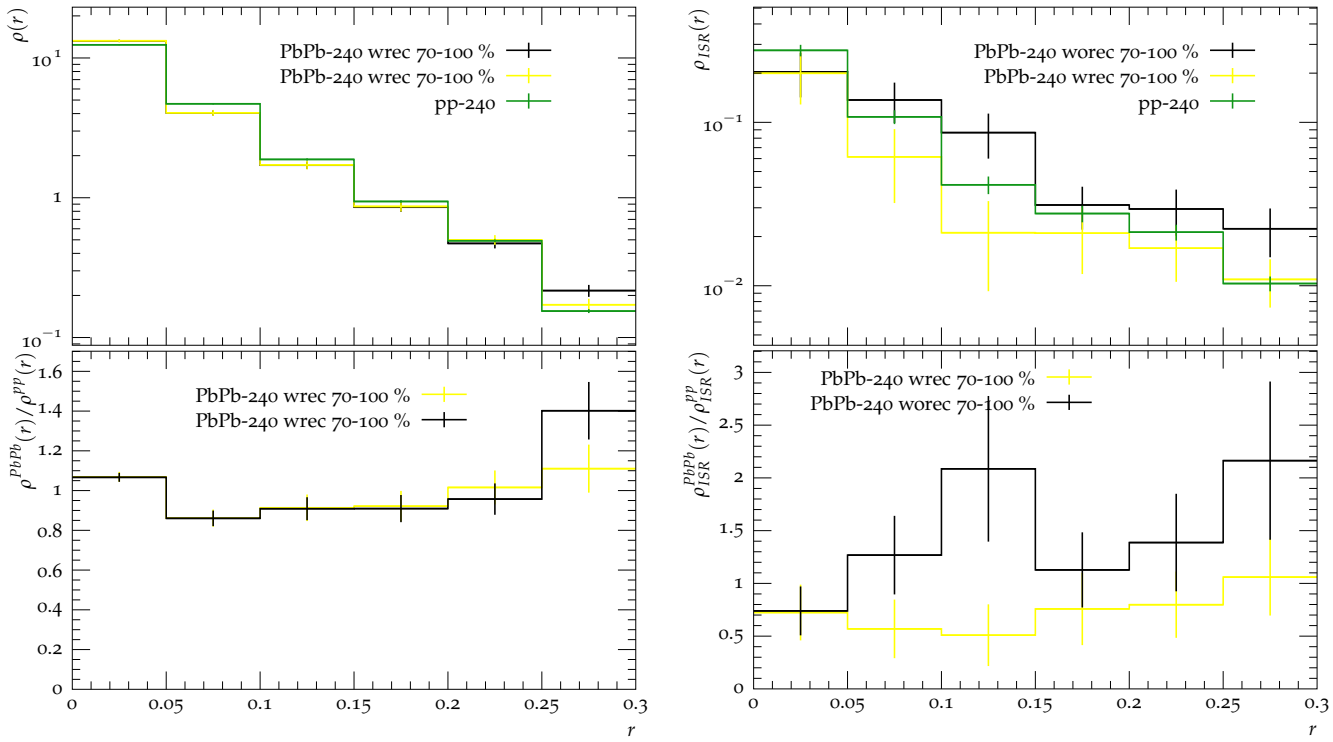

Figure 30: The jet-shape and ISR jet-shape are plotted in top figures, whereas the jet shape nuclear modification factors are plotted in the bottom figures for different distances r from the jet axis.

References

[1] E. D. Bloom, D. H. Coward, H. C. DeStaebler, J. Drees, G. Miller, L. W. Mo, R. E. Taylor, M. Breidenbach, J. I. Friedman and G. C. Hartmann, *et al.* "High-Energy Inelastic e p Scattering at 6-Degrees and 10-Degrees," Phys. Rev. Lett. **23** (1969), 930-934
doi:10.1103/PhysRevLett.23.930

[2] Report of the workshop on GeV/nucleon collisions of heavy ions: November 29-December 1, 1974, Bear Mountain, New York. United States
https://www.osti.gov/servlets/purl/4061527

[3] T. Ludlam *et al.*(2005) [BRAHMS, STAR, PHOBOS and PHENIX], "Hunting the quark gluon plasma,"
doi:10.2172/15015225

[4] P. Rosnet, (2015) "Quark-Gluon Plasma: from accelerator experiments to early Universe,"
arXiv:1510.04200[hep-ph]

[5] J. Rafelski, "Melting Hadrons, Boiling Quarks," Eur. Phys. J. A **51** (2015) no.9, 114
arXiv:1508.03260

[6] K. G. Wilson, "Confinement of Quarks," Phys. Rev. D **10** (1974), 2445-2459
doi:10.1103/PhysRevD.10.2445

[7] G. M. Prosperi, M. Raciti and C. Simolo, "On the running coupling constant in QCD," Prog. Part. Nucl. Phys. **58** (2007), 387-438
arXiv:hep-ph/0607209

[8] E. Martynov and B. Nicolescu, "Did TOTEM experiment discover the Odderon?," Phys. Lett. B **778** (2018), 414-418
arXiv:1711.03288[hep-ph]

[9] V. M. Abazov *et al.* [D0 and TOTEM], "Comparison of pp and $p\bar{p}$ differential elastic cross sections and observation of the exchange of a colorless C-odd gluonic compound,"
arXiv:2012.03981[hep-ex]

[10] M. N. Chernodub, "QCD string breaking in strong magnetic field," Mod. Phys. Lett. A **29** (2014), 1450162
arXiv:1001.0570[hep-ph]

[11] J. Adams *et al.* [STAR], "Experimental and theoretical challenges in the search for the quark gluon plasma: The STAR Collaboration's critical assessment of the evidence from RHIC collisions," Nucl. Phys. A **757** (2005), 102-183
arXiv:nucl-ex/0501009[nucl-ex]

[12] R. S. Bhalerao, "Relativistic heavy-ion collisions,"
arXiv:1404.3294[nucl-th]

[13] F. Karsch, "Lattice QCD at high temperature and density," Lect. Notes Phys. **583** (2002), 209-249
arXiv:hep-lat/0106019[hep-lat]

[14] S. Marzani, G. Soyez and M. Spannowsky, "Looking inside jets: an introduction to jet substructure and boosted-object phenomenology," Lect. Notes Phys. **958** (2019), pp.
arXiv:1901.10342[hep-ph]

[15] F. Bechtel, "The underlying event in proton-proton collisions," doi:10.3204/DESY-THESIS-2009-015

[16] G. P. Salam and G. Soyez, "A Practical Seedless Infrared-Safe Cone jet algorithm," JHEP **05** (2007), 086 arXiv:0704.0292[hep-ph]

[17] M. Cacciari, G. P. Salam and G. Soyez, JHEP **04** (2008), 063 arXiv:0802.1189[hep-ph]

[18] M. Cacciari and G. P. Salam, "Dispelling the N^3 myth for the k_t jet-finder," Phys. Lett. B **641** (2006), 57-61 arXiv:hep-ph/0512210[hep-ph]

[19] H. Satz, "Extreme states of matter in strong interaction physics. An introduction," Lect. Notes Phys. **841** (2012), 1-239 doi:10.1007/978-3-642-23908-3

[20] J. Casalderrey-Solana, J. G. Milhano and U. Wiedemann, "Jet quenching via jet collimation," J. Phys. G **38** (2011), 124086 arXiv:1107.1964[hep-ph]

[21] S. Chatrchyan *et al.* [CMS], "Modification of Jet Shapes in PbPb Collisions at $\sqrt{s_{NN}} = 2.76$ TeV," Phys. Lett. B **730** (2014), 243-263 arXiv:1310.0878[nucl-ex]

[22] R. J. Glauber and G. Matthiae, "High-energy scattering of protons by nuclei," Nucl. Phys. B **21** (1970), 135-157 doi:10.1016/0550-3213(70)90511-0

[23] R. Baier, "Jet quenching," Nucl. Phys. A **715** (2003), 209-218 arXiv:hep-ph/0209038[hep-ph]

[24] G. Y. Qin and X. N. Wang, "Jet quenching in high-energy heavy-ion collisions," Int. J. Mod. Phys. E **24** (2015) no.11, 1530014 arXiv:1511.00790[hep-ph]

[25] J. Adam *et al.* [ALICE], "Measurement of transverse energy at midrapidity in Pb-Pb collisions at $\sqrt{s_{\rm NN}} = 2.76$ TeV," Phys. Rev. C **94** (2016) no.3, 034903 arXiv:1603.04775[nucl-ex]

[26] B. Abelev *et al.* [ALICE], "Centrality determination of Pb-Pb collisions at $\sqrt{s_{NN}} = 2.76$ TeV with ALICE," Phys. Rev. C **88** (2013) no.4, 044909 arXiv:1301.4361[nucl-ex]

[27] S. Sumowidagdo, "Experimental study of matter under the influence non-abelian gauge theory," J. Phys. Conf. Ser. **856** (2017) no.1, 012002 doi:10.1088/1742-6596/856/1/012002

[28] C. Gale, S. Jeon and B. Schenke, "Hydrodynamic Modeling of Heavy-Ion Collisions," Int. J. Mod. Phys. A **28** (2013), 1340011 arXiv:1301.5893[nucl-th]

[29] J. Xu and C. M. Ko, "Chemical freeze-out in relativistic heavy-ion collisions," Phys. Lett. B **772** (2017), 290-293 doi:10.1016/j.physletb.2017.06.061 arXiv:1704.04934[nucl-th]

[30] K. C. Zapp, "JEWEL 2.0.0: directions for use," Eur. Phys. J. C **74** (2014) no.2, 2762 doi:10.1140/epjc/s10052-014-2762-1
arXiv:1311.0048[hep-ph]

[31] T. Sjostrand, S. Mrenna and P. Z. Skands, "PYTHIA 6.4 Physics and Manual," JHEP **05** (2006), 026
arXiv:hep-ph/0603175[hep-ph]

[32] M. R. Whalley, D. Bourilkov and R. C. Group, "The Les Houches accord PDFs (LHAPDF) and LHAGLUE,"
arXiv:hep-ph/0508110[hep-ph]

[33] M. Cacciari, G. P. Salam and G. Soyez, "FastJet User Manual," Eur. Phys. J. C **72** (2012), 1896
arXiv:1111.6097[hep-ph]

[34] A. Buckley, J. Butterworth, D. Grellscheid, H. Hoeth, L. Lonnblad, J. Monk, H. Schulz and F. Siegert, "Rivet user manual," Comput. Phys. Commun. **184** (2013), 2803-2819
arXiv:1003.0694[hep-ph]

[35] K. Zapp, G. Ingelman, J. Rathsman, J. Stachel and U. A. Wiedemann, "A Monte Carlo Model for 'Jet Quenching'," Eur. Phys. J. C **60** (2009)
arXiv:0804.3568[hep-ph]

[36] B. Andersson, G. Gustafson, G. Ingelman and T. Sjostrand, "Parton Fragmentation and String Dynamics," Phys. Rept. **97** (1983), 31-145
doi:10.1016/0370-1573(83)90080-7

[37] P. Berta, M. Spousta, D. W. Miller and R. Leitner, "Particle-level pileup subtraction for jets and jet shapes," JHEP **06** (2014)
arXiv:1403.3108[hep-ex]

[38] G. Milhano and K. Zapp, in preparation.